Inorganic Chemistry

pubs.acs.org/IC

Article

Effect of *N,N* Coordination and Ru^{II} Halide Bond in Enhancing Selective Toxicity of a Tyramine-Based Ru^{II} (*p*-Cymene) Complex

Arpan Mukherjee,[§] Sourav Acharya,[§] Kallol Purkait, Kaustav Chakraborty, Ashima Bhattacharjee, and Arindam Mukherjee*

Cite This: https://dx.doi.org/10.1021/acs.inorgchem.0c00694

Read Online

ACCESS | Metrics & More | Article Recommendations | Supporting Information

ABSTRACT: Ruthenium compounds are promising anticancer candidates owing to their lower side-effects and encouraging activities against resistant tumors. Half-sandwich piano-stool type Ru^{II} compounds of general formula $[(L)Ru^{II}(\eta^6\text{-arene})(X)]^+$ (L = chelating bidentate ligand, X = halide) have exhibited significant therapeutic potential against cisplatin-resistant tumor cell lines. In Ru^{II} (*p*-cymene) based complexes, the change of the halide leaving group has led to several interesting features, viz., hydrolytic stability, resistance toward thiols, and alteration in pathways of action. Tyramine is a naturally occurring monoamine which acts as a catecholamine precursor in humans. We synthesized a family of *N,N* and *N,O* coordinated Ru^{II} (*p*-cymene) complexes, $[(L)\text{-}Ru^{II}(\eta^6\text{-arene})(X)]^+$ (**1**−**4**), with tyramine and varied the halide (X = Cl, I) to investigate the difference in reactivity. Our studies showed that complex **2** bearing *N,N* coordination with an iodido leaving group shows selective *in vitro* cytotoxicity against the pancreatic cancer cell line MIA PaCa-2 (IC_{50} ca. 5 μM) but is less toxic to triple-negative breast cancer (MDA-MB-231), hepatocellular carcinoma (Hep G2), and the normal human foreskin fibroblasts (HFF-1). Complex **2** displays stability toward hydrolysis and does not bind with glutathione, as confirmed by ^{1}H NMR and ESI-HRMS experiments. The inert nature of **2** leads to enhancement of cytotoxicity (IC_{50} = 5.3 ± 1 μM) upon increasing the cellular treatment time from 48 to 72 h.

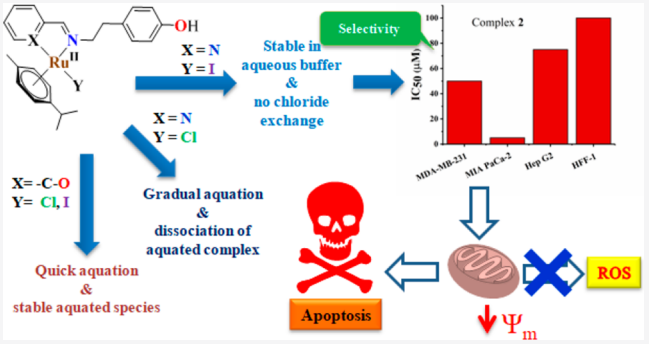

INTRODUCTION

Cancer, a globally threatening disease, takes a major toll on human life every year.[1] The growing resistance of cancer toward existing chemotherapeutics[2−5] including Pt-based drugs have led to new Pt and non-Pt metal complexes.[6−28] In this regard, the Ru(II/III) complexes have shown promise owing to their lower side-effects and encouraging activities,[18] viz., targeting DNA or protiens,[8,9,13,14,16,22,23,26] accumulation in various cellular organelles and enhancement of oxidative stress,[6,12,25,27] photoactivation,[10] higher cytotoxicity to cancer cells,[11,17,19] and disruption of the cellular redox balance.[20,21,24,28] Several Ru complexes like NAMI-A, NKP-1339, and TLD1433 have been to clinical trials (Figure 1).[29−34] Ru^{III} complexes can act as "pro-drugs," that display kinetic inertness and can be reduced to Ru^{II} in physiology.[35] Half-sandwich piano-stool type Ru^{II} compounds of general formula $[(YZ)Ru^{II}(\eta^6\text{-arene})(X)]^+$ (YZ = chelating bidentate ligand, X = halide) exhibit significant therapeutic potential against cisplatin-resistant tumor cell lines,[36−40,3,5,41−43] and several of them, viz., RM175, RAPTA-C, and RAPTA-T (Figure 1), have undergone pre-clinical trials.[5,44−46] The aquated Ru^{II} complexes display ligand exchange kinetics which may differ from or be similar to Pt^{II} drugs.[47] In this class of complexes, a change of the halide leaving group leads to a change in kinetic inertness and also alters the mechanism of action in many cases.[48−52]

In this work, we have selected tyramine, a naturally occurring monoamine that acts as a catecholamine precursor, as part of a bidentate ligand.[53] Tyramine is part of our physiological system and can be metabolized by monoamine oxidase.[54,55] Schiff base derivatives of tyramine with pyridine-2-carbaldehyde have been previously reported.[56−59] They have been utilized for developing Cu^{II}-conjugated phosphorus dendrimers bearing a cyclotriphosphazene core and also showed antitumoral/antimicrobial activities as dual Au^{III}−Cu^{II} conjugated dendrimers.[56−58] The Au^{III}−Cu^{II} conjugated dendrimers designed exhibited cytotoxicity in the range 3−600 nM against epithelial carcinoma (KB) and promyelocytic leukemia (HL60) cell lines.[59] The corresponding Cu^{II} and Ni^{II} complexes were investigated for inhibition of urease and xanthine oxidase.[60] In a recent study,

Received: March 6, 2020

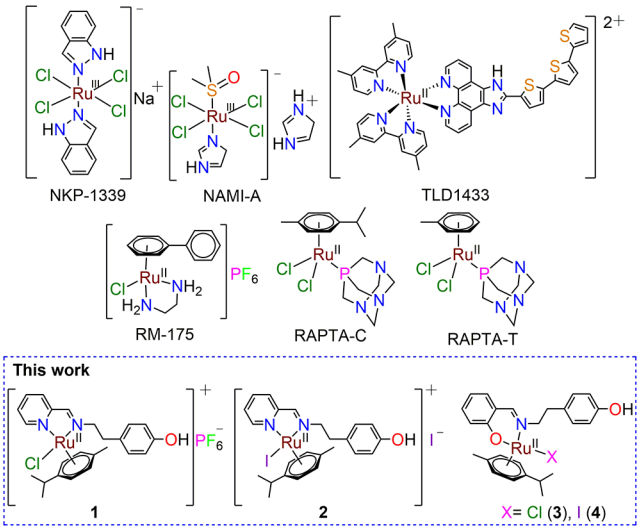

Figure 1. Representation of Ru^{III} (NKP-1339 and NAMI-A), organometallic half-sandwich Ru^{II} (RM-175, RAPTA-C, and RAPTA-T), and polypyridyl Ru^{II} (TLD1433) anticancer agents, along with the *p*-cymene based Ru^{II} complexes studied in this work.

Co^{II} complexes of similar ligands have displayed electrochemical hydrogen evolution at pH < 4.[61] Hence, the ligands used are known for their activity against various proteins depending on the metal ions used. The work presented here involves Ru^{II}(*p*-cymene) complexes (**1**−**4**) of tyramine based Schiff bases with pyridine-2-carbaldehyde and salicylaldehyde (L1, L2) leading to variation in the coordination from *N,N* to *N,O*. In addition the kinetic stability was also altered with variation of the halide (X = Cl, I) and the aldehyde. All the four complexes were well characterized by various analytical techniques like FT-IR, UV−visible spectroscopy, ^{1}H NMR, ^{13}C NMR, and ESI-HRMS. The structures of **1** and **2** were confirmed by single crystal X-ray diffraction. Bulk purity was confirmed by elemental analysis. Activities of **1**−**4** were probed *in vitro* against a panel of three different carcinoma cell lines (MDA-MB-231, triple-negative breast adenocarcinoma; Hep G2, hepatocellular carcinoma; and MIA PaCa-2, pancreas ductal adenocarcinoma). The stability of the complexes in solution varied based on the ligands used, and it also influenced their cytotoxicity.

EXPERIMENTAL SECTION

Materials and Methods. All chemicals and solvents were purchased from commercial sources. Solvents were distilled and dried prior to use by standard procedures.[62] Pyridine 2-carbaldehyde, salicylaldehyde, and reduced L-glutathione were purchased from Sigma-Aldrich and used without any further purification. Tyramine monohydrochloride was purchased from Spectrochem, India. Ruthenium(III) trichloride was purchased from Precious Metals Online, Australia. $[Ru^{II}(\eta^6\text{-}p\text{-cymene})Cl_2]_2$ was prepared using a literature protocol.[63] MTT [3-(4,5-dimethylthiazol-2-yl)-2,5-diphenyl-tetrazolium bromide] (USB), along with supplements and assay kits, were purchased from Gibco and used as received. UV−visible measurements were done using an Agilent Cary 300 UV−vis spectrophotometer. FT-IR spectra were recorded using a PerkinElmer SPECTRUM RX I spectrometer in KBr pellets. ^{1}H and proton decoupled ^{13}C NMR spectra were measured using either a JEOL ECS 400 MHz or Bruker Avance III 500 MHz spectrometer at room temperature. The chemical shifts are reported in parts per million (ppm). Electro-spray ionization mass spectra were recorded using a Bruker maXis impact mass spectrometer by positive mode of electrospray ionization. The synthetic yields reported are of isolated analytically pure compounds. The ligands and complexes synthesized were dried in a vacuum and stored in a desiccator in the dark.

Syntheses. *Synthesis of 4-(2-(Pyridin-2-ylmethyleneamino)-ethyl)phenol (L1).* To a stirred solution of tyramine monohydrochloride (0.2 g, 1.15 mmol) in MeOH, LiOH (0.04 g, 1.15 mmol) was added. The mixture was allowed to stir for 1 h and placed under ice. Pyridine-2-carbaldehyde (0.123 g, 1.15 mmol) was added dropwise to the above solution over a period of 15 min. The resulting solution was allowed to stir at room temperature for 12 h. The solvent was evaporated under reduced pressure, and the obtained crude product was washed two times with petroleum ether, yielding a yellowish-white solid. Yield: 85%. ^{1}H NMR (500 MHz, DMSO-d_6): δ 9.17 (s, 1H, −OH), 8.61 (d, 1H, J = 4.45 Hz, Py-H), 8.22 (s, 1H, −CH═N), 7.94 (d, 1H, J = 7.85 Hz, Py-H), 7.88 (t, 1H, J = 7.62 Hz, Py-H), 7.46 (t, 1H, J = 6.1 Hz, Py-H), 7.03 (d, 2H, J = 8.3 Hz, Ar−H), 6.66 (d, 2H, J = 8.3 Hz, Ar−H), 3.82 (t, 2H, J = 7.17 Hz, $-CH_2$), 2.83 (t, 2H, J = 7.27 Hz, $-CH_2$) (Supporting Information, Figure S1). ^{13}C NMR (125 MHz, DMSO-d_6, 25 °C): δ 161.9, 155.9, 154.2, 149.4, 137.0, 129.6, 125.1, 120.5, 115.5, 115.2, 62.3, 35.9 (Supporting Information, Figure S2).

Synthesis of 2-(((4-Hydroxyphenethyl)imino)methyl)phenol (L2). To a stirred solution of tyramine monohydrochloride (0.2 g, 1.15 mmol) in MeOH, LiOH (0.04 g, 1.15 mmol) was added. The mixture was allowed to stir for 1 h. Salicylaldehyde (0.140 g, 1.15 mmol) was added dropwise to the above solution and allowed to stir at rt for 12 h. The solvent was evaporated under reduced pressure, and the obtained crude was washed repeatedly with petroleum ether, yielding a bright yellow solid. Yield: 83%. ^{1}H NMR (500 MHz, DMSO-d_6): δ 13.53 (s, 1H, Sal−OH), 9.24 (s, 1H, Ar−OH), 8.45 (s, 1H, −CH═N), 7.38 (d, 1H, J = 9.3 Hz, Sal-H), 7.32 (t, 1H, J = 10.1 Hz, Sal-H), 7.03 (d, 2H, J = 10.35 Hz, Ar−H), 6.87 (t, 2H, J = 9.15 Hz, Sal-H), 6.68 (d, 2H, J = 10.4 Hz, Ar−H), 3.79 (t, 2H, J = 8.62 Hz, $-CH_2$), 2.84 (t, 2H, J = 8.72 Hz, $-CH_2$) (Supporting Information, Figure S3). ^{13}C NMR (125 MHz, DMSO-d_6, 25 °C): δ 165.8, 161.0, 155.7, 154.4, 132.3, 131.6, 129.6, 129.2, 118.6, 118.3, 116.6, 115.2, 60.0, 35.9 (Supporting Information, Figure S4).

*$[(L1)Ru^{II}(\eta^6\text{-}p\text{-cym})(Cl)](PF_6)$ (**1**).* To a solution of L1 (0.1 g, 0.44 mmol), dissolved in 10 mL of methanol, a 10 mL methanolic solution of $[Ru^{II}(\eta^6\text{-}p\text{-cymene})Cl_2]_2$(0.130 g, 0.22 mmol) was added under stirring conditions. The whole reaction mixture was allowed to reflux for 4 h, followed by the addition of NH_4PF_6 (0.087 g, 0.53 mmol), dissolved in ca. 5 mL of methanol. The solvent was evaporated under reduced pressure, extracted with dichloromethane, and re-evaporated. The resulting orange colored crude product was washed with chilled diethyl ether multiple times. The pure product was isolated as a yellow powder, which was soluble in methanol, ethanol, acetonitrile, and DMSO. Yield: 0.179 g (64%). Anal. Calcd for $C_{24}H_{28}ClF_6N_2OPRu$: C,44.90; H, 4.40; N, 4.36. Found: C, 44.67; H, 4.31; N, 4.41. ^{1}H NMR (500 MHz, DMSO-d_6): δ 9.53 (d, 1H, J = 4.32 Hz, Py-H), 8.67 (s, 1H, −CH═N), 8.25 (t, 1H, J = 6.12 Hz, Py-H), 8.14 (d, 1H, J = 6.04 Hz, Py-H), 7.82 (t, 2H, J = 5.24 Hz, Py-H), 7.19 (d, 2H, J = 6.68 Hz, Ar−H), 6.74 (d, 2H, J = 6.68 Hz, Ar−H), 6.29 (d, 1H, J = 5.04 Hz, *p*-cym-H), 6.21 (d, 1H, J = 4.88 Hz, *p*-cym-H), 5.97 (d, 1H, J = 4.88 Hz, *p*-cym-H), 5.92 (d, 1H, J = 5.04 Hz, *p*-cym-H), 4.65 (m, 1H, $-CH_2$), 4.54 (m, 1H, $-CH_2$), 3.21 (m, 1H, $-CH_2$), 2.93 (m, 1H, $-CH_2$), 2.62 (m, 1H, *p*-cym-CH), 2.18 (s, 3H, *p*-cym-CH_3), 1.03 (d, 3H, J = 5.52 Hz, iPr-CH_3), 0.94 (d, 3H, J = 5.52 Hz, iPr-CH_3) (Supporting Information, Figure S5). ^{13}C NMR (125 MHz, DMSO-d_6, 25 °C): δ 167.3, 156.0, 155.8, 154.4, 139.8, 130.0, 128.6, 128.2, 127.8, 115.2, 104.5, 103.2, 87.3, 84.9, 84.7, 84.3, 67.4, 34.6, 30.4, 22.0, 21.4, 18.3 (Supporting Information, Figure S6). FT-IR (KBr pellets, cm^{-1}): 3541, 2970, 1613, 1515, 1261, 1202, 836, 553. UV−vis [CH_3OH, λ_{max}, nm (ε/dm^3 mol^{-1} cm^{-1})]: 271 (6600), 350 (2530), 406 (1820). ESI-HRMS (methanol) m/z (calcd): 497.0928 (497.0744) [$C_{24}H_{28}ClN_2ORu^+$].

*$[(L1)Ru^{II}(\eta^6\text{-}p\text{-cym})(I)](I)$ (**2**).* To a solution of L1 (0.08 g, 0.35 mmol), dissolved in 10 mL of methanol under stirring conditions, $[Ru^{II}(\eta^6\text{-}p\text{-cymene})I_2]_2$ (0.173 g, 0.17 mmol) dissolved in 10 mL of methanol was added. The whole reaction mixture was allowed to reflux for 5 h. The solvent was evaporated under reduced pressure, extracted with dichloromethane, and re-evaporated. The resulting deep orange crude was washed with chilled diethyl ether for purification. The pure

https://dx.doi.org/10.1021/acs.inorgchem.0c00694
Inorg. Chem. XXXX, XXX, XXX−XXX

Table 1. Selected Crystallographic Parameters of Complexes 1 and 2

	1	2
empirical formula	$C_{24}H_{28}ClF_6N_2OPRu$	$C_{24}H_{28}I_2N_2ORu$
radiation	Mo Kα (λ = 0.71073)	Mo Kα (λ = 0.71073)
formula weight	641.99	715.35
temperature (K)	100.00(10)	178(100)
crystal system	orthorhombic	monoclinic
space group	$P2_12_12_1$	$P2_1/c$
a (Å)	38.570(4)	10.2017(3)
b (Å)	16.2804(9)	14.4742(3)
c (Å)	7.7893(3)	17.2490(5)
α (deg.)	90.00	90.00
β (deg.)	90.00	100.885(3)
γ (deg.)	90.00	90.00
volume (Å^3)	4891.2(6)	2501.18(12)
Z	4	4
calculated density (mg/m^3)	1.744	1.900
F(000)	2592.0	1376.0
μ/mm^{-1}	0.884	3.113
goodness-of-fit on F^2	1.149	1.053
final R indices [$I > 2\sigma(I)$]	R_1 = 0.0426, wR_2 = 0.0882	[a]R_1 = 0.0208,[b] wR_2 = 0.0517
R_{int}	0.0389	0.0306
R_{sigma}	0.0662	0.0266

[a]$R_1 = \sum||F_o| - |F_c||/\sum|F_o|$. [b]$wR_2 = [\sum[w(F_o^2 - F_c^2)^2]/\sum w[(F_o^2)^2]]^{1/2}$.

product was obtained as a reddish-brown solid which was soluble in methanol, ethanol, acetonitrile, and DMSO. Yield: 0.175 g (70%). Anal. Calcd for $C_{24}H_{28}I_2N_2ORu$: C, 40.30; H, 3.95; N, 3.92. Found: C, 40.11; H, 3.89; N, 4.01. ^{1}H NMR (500 MHz, DMSO-d_6): δ 9.51 (d, 1H, J = 4.4 Hz, Py-H), 9.33 (s, 1H, −OH), 8.66 (s, 1H, −CH═N), 8.23 (m, 2H, Py-H), 7.76 (t, 1H, J = 5.88 Hz, Py-H), 7.21 (d, 2H, J = 6.72 Hz, Ar−H), 6.76 (d, 2H, J = 6.68 Hz, Ar−H), 6.17 (t, 2H, J = 6 Hz, p-cym-H), 5.97 (t, 2H, J = 4.9 Hz, p-cym-H), 4.55 (m, 2H, −CH$_2$), 3.23 (m, 1H, −CH$_2$), 3.07 (m, 1H, −CH$_2$), 2.72 (m, 1H, p-cym-CH), 2.39 (s, 3H, p-cym-CH$_3$), 1.07 (d, 3H, J = 5.32 Hz, iPr-CH$_3$), 0.90 (d, 3H, J = 5.52 Hz, iPr-CH$_3$) (Supporting Information, Figure S8). ^{13}C NMR (125 MHz, DMSO-d_6, 25 °C): δ 166.6, 157.1, 156.1, 154.4, 139.5, 129.9, 128.9, 127.8, 127.6, 115.3, 107.0, 101.6, 86.6, 85.8, 85.3, 84.7, 68.1, 35.7, 31.0, 21.9, 21.3, 20.0 (Supporting Information, Figure S9). FT-IR (KBr pellets, cm^{-1}): 3534, 2964, 1616, 1514, 1262, 1207, 836, 557. UV−vis [CH$_3$OH, λ_{max}, nm (ε/dm^3 mol^{-1} cm^{-1})]: 223 (27600), 272 (8700), 365 (2800), 437 (1480). ESI-HRMS (methanol) m/z (calcd): 589.0284 (589.0261) [$C_{24}H_{28}IN_2ORu^+$].

*[(L2)Ru^{II}(η^6-p-cym)(Cl)] (**3**).* To a solution of L2 (0.1 g, 0.41 mmol), dissolved in 10 mL of methanol, KOH (0.09 g, 0.373 mmol) and [Ru^{II}(η^6-p-cymene)Cl$_2$]$_2$ (0.127 g, 0.207 mmol), also dissolved in methanol, were added subsequently. The whole reaction mixture was allowed to stir at 25 °C for 12 h. The solvent was filtered and evaporated under reduced pressure, and the resulting orange crude was extracted with DCM. The DCM layer was evaporated under reduced pressure and washed two times with chilled diethyl ether to obtain a reddish-brown crude. The crude was purified by means of column chromatography, packed with neutral alumina, using 0.1% MeOH in DCM as an eluent. Product was isolated as a reddish-orange powder. Yield: 0.156 g (74%). Anal. Calcd for $C_{25}H_{28}ClNO_2Ru$: C, 58.76; H, 5.52; N, 2.74. Found: C, 58.94; H, 5.50; N, 2.68. ^{1}H NMR (500 MHz, CDCl$_3$): δ 7.51 (s, 1H, −CH═N), 7.17 (m, 3H, Sal-H and Ar−H), 6.96 (d, 1H, J = 8.52 Hz, Sal-H), 6.81 (m, 3H, Sal-H and Ar−H), 6.41 (t, 1H, J = 7.26 Hz, Sal-H), 5.40 (s, 2H, p-cym-H), 5.36 (d, 1H, J = 5.68 Hz, p-cym-H), 5.06 (d, 1H, J = 5.64 Hz, p-cym-H), 4.47 (m, 1H, −CH$_2$), 4.23 (m, 1H, −CH$_2$), 3.32 (m, 1H, −CH$_2$), 3.16 (m, 1H, −CH$_2$), 2.79 (m, 1H, p-cym-CH), 2.23 (s, 3H, p-cym-CH$_3$), 1.24 (d, 3H, J = 6.92 Hz, iPr-CH$_3$), 1.14 (d, 3H, J = 6.88 Hz, iPr-CH$_3$) (Supporting Information, Figure S11). ^{13}C NMR (125 MHz, CDCl$_3$, 25 °C): δ 164.6, 164.2, 155.3, 134.9, 134.5, 130.0, 129.9, 122.1, 119.6, 116.1, 114.7, 101.9, 97.8, 85.7, 83.2, 81.9, 80.6, 70.0, 36.6, 30.7, 22.8, 21.9, 18.8 (Supporting Information, Figure S12). FT-IR (KBr pellets, cm^{-1}): 3406, 2964, 2925, 1620, 1518, 1449, 1318, 1233, 754. UV−vis: [CH$_3$OH, λ_{max}, nm (ε/dm^3 mol^{-1} cm^{-1})]: 226 (68050), 284 (19700), 384 (6250), 487 (1700). ESI-HRMS (methanol) m/z (calcd): 476.1158 (476.1135) [$C_{25}H_{28}NO_2Ru^+$]

*[(L2)Ru^{II}(η^6-p-cym)(I)] (**4**).* Compound **4** was prepared following a procedure similar to that reported for **3**, starting from L2 (0.08 g, 0.331 mmol), KOH (0.016 g, 0.298 mmol), and [Ru^{II}(η^6-p-cymene)I$_2$]$_2$ (0.162 g, 0.165 mmol). Product was obtained as a deep brown solid after column chromatography, packed with neutral alumina, using 0.1% MeOH in DCM as an eluent. Yield: 0.122 g (61%). Anal. Calcd for $C_{25}H_{28}INO_2Ru$: C, 49.84; H, 4.68; N, 2.32. Found: C, 49.49; H, 4.43; N, 2.45. ^{1}H NMR (500 MHz, DMSO-d_6): δ 9.31 (s, 1H, −OH), 8.36 (s, 1H, −CH═N), 7.27 (m, 2H, Sal-H), 7.18 (d, 2H, J = 8.36 Hz, Ar−H), 6.87 (d, 1H, J = 8.4 Hz, Sal-H), 6.75 (d, 2H, J = 8.36 Hz, Ar−H), 6.60 (t, 1H, J = 7.32 Hz, Sal-H), 6.01 (br.s, 4H, p-cym-H), 4.35 (t, 2H, J = 6.94 Hz, −CH$_2$), 3.11 (t, 2H, J = 7.02 Hz, −CH$_2$), 2.55 (m, 1H, p-cym-CH), 2.08 (s, 3H, p-cym-CH$_3$), 1.07 (d, 6H, J = 5.56 Hz, p-cym-iPr-CH$_3$) (Supporting Information, Figure S14). ^{13}C NMR (125 MHz, DMSO-d_6, 25 °C): δ 155.9, 135.0, 134.5, 129.8, 128.7, 128.1, 126.0, 121.5, 119.9, 115.1, 114.9, 84.8, 83.2, 80.1, 77.5, 70.6, 66.5, 66.3, 35.9, 30.1, 23.9, 21.3 (Supporting Information, Figure S15). FT-IR (KBr pellets, cm^{-1}): 3410, 2964, 1616, 1518, 1449, 1325, 1200, 767. UV−vis [CH$_3$OH, λ_{max}, nm (ε/dm^3 mol^{-1} cm^{-1})]: 222 (29800), 286 (6020), 393 (1940), 484 (560). ESI-HRMS (Methanol) m/z (calcd): 476.1158 (476.1135) [$C_{25}H_{28}NO_2Ru^+$]

X-ray Crystallography. Good quality single crystals suitable for X-ray diffraction were obtained by layering acetonitrile solutions of the isolated complexes (**1** and **2**) with diethyl ether. Single crystals were mounted using loops on the goniometer head of a SuperNova, Dual, Cu at zero, Eos diffractometer (Agilent) equipped with graphite monochromated Mo Kα radiation (0.71073 Å) and data collected at 100 K. An empirical multiscan absorption correction was performed using SADABS. The structures were solved by direct methods, and all non-hydrogen atoms were refined anisotropically by full matrix least-squares on F^2. A few important crystallographic refined parameters are summarized in Table 1 and Table 2. The hydrogen atoms were calculated and fixed using riding model SHELXL-97 after hybridization of all non-hydrogen atoms. The CCDC numbers are 1969294 for complex **1** and 1969295 for complex **2**.

https://dx.doi.org/10.1021/acs.inorgchem.0c00694
Inorg. Chem. XXXX, XXX, XXX−XXX

Table 2. Selected Bond Lengths (Å) and Bond Angles (deg) for Complexes 1 and 2

1		2	
Ru1 Cl1 2.394(2)	N2 Ru1 N1 76.4(2)	Ru1 I1 2.7174(3)	N1 Ru1 N2 76.89(9)
Ru1 N1 2.069(6)	N1 Ru1 Cl1 86.76(17)	Ru1 N1 2.069(2)	N1 Ru1I1 85.62(6)
Ru1 N2 2.065(6)	N2 Ru1 Cl1 83.05(17)	Ru1 N2 2.064(2)	N2 Ru1 I1 85.82(6)
Ru1 C15 2.210(7)	N2 Ru1 C15 119.5(3)	Ru1 C15 2.205(3)	N1 Ru1 C15 94.53(10)
Ru1 C16 2.163(7)	N2 Ru1 C16 95.9(3)	Ru1 C16 2.186(3)	N1 Ru1 C16 121.36(10)
Ru1 C17 2.185(7)	N2 Ru1 C17 97.6(3)	Ru1 C17 2.215(3)	N1 Ru1 C17 158.99(10)
Ru1 C18 2.245(8)	N2 Ru1 C18 121.7(3)	Ru1 C18 2.247(3)	N1 Ru1 C18 155.92(10)
Ru1 C19 2.196(8)	N2 Ru1 C19 159.5(3)	Ru1 C19 2.219(3)	N1 Ru1 C19 118.99(10)
Ru1 C20 2.190(7)	N2 Ru1 C20 157.2(2)	Ru1 C20 2.201(3)	N1 Ru1 C20 94.76(10)
	N1 Ru1 C15 92.7(3)		N2 Ru1 C15 113.52(10)
	N1 Ru1 C16 117.1(3)		N2 Ru1 C16 92.62(10)
	N1 Ru1 C17 154.2(3)		N2 Ru1 C17 99.13(10)
	N1 Ru1 C18 161.5(3)		N2 Ru1 C18 126.70(11)
	N1 Ru1 C19 123.7(3)		N2 Ru1 C19 164.12(10)
	N1 Ru1 C20 97.2(3)		N2 Ru1 C20 150.39(10)

Stability Studies. The complexes were dissolved in a mixture of DMSO-d_6 and 10 mM PBS buffer (pD = 7.4) containing 4 mM NaCl (3:7 v/v), and the spectra were recorded by ^{1}H NMR at 25 °C at different time intervals. The UV−visible spectral study of complexes **1** and **2** was also performed via UV−visible spectroscopy using 1:9 (v/v) methanol/PBS buffer with 4 mM NaCl at pH = 7.4.

The stability studies of the complexes in ESI-MS were performed using micromolar solutions of the complexes in methanol and 10 mM PBS buffer (pH = 7.4) containing both 4 and 130 mM NaCl (2:8 v/v) at 25 °C. The data were analyzed and plotted using Bruker Daltonics software.

The stability of complex **2** in extracellular chloride concentration (130 mM) was determined by ^{1}H NMR at 25 °C. Briefly, 1.2 mg of the sample was dissolved in 600 μL of 3:7 (v/v) DMSO-d_6/10 mM PBS buffer (pD = 7.4) containing 130 mM NaCl. The spectra were recorded up to 24 h.

Binding Studies with Model Nucleobase 9-Ethylguanine (9-EtG). One molar equivalent of the complexes was coincubated with 2 mol equiv of 9-EtG in a 3:7 v/v DMSO-d_6/10 mM PBS buffer (pD = 7.4) containing 4 mM NaCl, and the spectra were recorded at 25 °C by ^{1}H NMR for 24 h at different time intervals. The ESI-MS studies were done using a 1:5 ratio of the complexes with respect to 9-EtG in a 2:8 v/v mixture of methanol and 10 mM PBS buffer (pH = 7.4) containing 4 mM NaCl at 25 °C. The data were analyzed and plotted using Bruker Daltonics software.

Binding Studies with L-Glutathione (GSH). The complexes were used for binding studies with reduced L-glutathione using ^{1}H NMR. Complexes were dissolved in a degassed mixture of 3:7 v/v DMSO-d_6 and 10 mM PBS buffer (pD = 7.4) containing 4 mM NaCl at 25 °C and under a nitrogen atmosphere for the purpose of minimizing the auto-oxidation of glutathione. Each experiment involved one molar equivalent of the complex coincubated with 2 mol equiv of GSH in the above solution. The spectra were recorded for 24 h at different time intervals.

In the case of GSH binding studies by means of ESI-MS, the solutions were a 2:8 (v/v) mixture of methanol and 10 mM PBS buffer (pH = 7.4) containing 4 mM NaCl. Each experiment involved one molar equivalent of the complex coincubated with 5 mol equiv of GSH in the above solution at 25 °C. The data were analyzed and plotted using Bruker Daltonics software.

Distribution Coefficient Determination. The distribution coefficient (log D) was determined using the traditional shake-flask method using octanol-10 mM phosphate buffer (pH = 7.4). After pre-equilibration of octanol and aqueous phosphate buffer (2 mL each) overnight, **1**−**4** (1 mg each) were added and shaken continuously (150 rpm) at 37 °C for 6 h on a shaker. The tubes were then centrifuged and aliquots of the octanol and aqueous buffer layers were pipetted out separately. Absorbances were measured, with necessary dilutions, by means of UV−visible spectroscopy. Each set was performed in triplicate. Concentration in each layer was determined from the respective molar extinction coefficient values, and the corresponding distribution coefficient (log D) was calculated.

Cell Lines and Culture Condition. Triple negative human metastatic breast adenocarcinoma (MDA-MB-231), hepatocellular carcinoma (Hep G2), and human pancreatic carcinoma (MIA PaCa-2) were bought from NCCS, Pune, India. Normal human foreskin fibroblasts (HFF-1) were purchased from ATCC. Cell lines were maintained in the logarithmic phase at 37 °C in a 5% carbon dioxide atmosphere using a suitable culture medium, 10% fetal bovine serum (GIBCO), and 1% antibiotic−antimycotic solution.

Cell Viability Assay. The growth inhibitory effect toward MDA-MB-231, Hep G2, and MIA PaCa-2 tumor cell lines was evaluated with the help of MTT assay. In brief, 6×10^3 cells per well were seeded in 96-well microplates in the medium (200 μL) and incubated at 37 °C in a 5% carbon dioxide atmosphere. After 24 h, the medium was renewed with a fresh one (200 μL). Stock solutions of **1**−**4** in DMSO−medium mixture were made immediately prior to drug dilution. Various concentrations of solution were prepared from the stock solution diluted with the same culture medium within 5 min and added in triplicate to attain appropriate concentrations in the respective wells. The final DMSO concentration in wells did not exceed 0.2% for the complexes. The same amount of DMSO percentage was maintained in the case of all cell based studies mentioned below. Upon completion of 72 h of incubation with the compounds, fresh medium (200 μL) was added to each well after removing the drug containing medium followed by treatment with 20 μL of a 1 mg mL^{-1} MTT in 1× PBS (pH = 7.2). After 3 h of incubation at 37 °C, medium was removed, and the resulting formazan crystals were dissolved in spectroscopy grade DMSO (200 μL). The growth inhibition of the cells was analyzed by comparing the absorbance of the drug treated wells with respect to untreated ones at 570 nm using either a BIOTEK ELx800 or a SpectraMax M2e plate reader. IC_{50} values (drug concentrations that is responsible for 50% cell growth inhibition) were calculated by fitting nonlinear curves (using four parameter fitting) in GraphPad Prism 5, using a variable slope model constructed by plotting cell viability (%) versus the log of drug concentration in micromoles. Each independent experiment was carried out in triplicate.

Cell Cycle Arrest. A total of 5×10^4 MIA PaCa-2 cells were cultured in 100 mm sterile cell culture Petri dishes suspended in 5 mL of DMEM under previously described culturing conditions. After 48 h, the medium was removed and replenished with fresh medium. A 35 μM concentration of **2** was added and incubated under the same conditions described above. After being exposed to **2** for 16 h, cells were harvested by trypsinization, centrifuged, and washed twice with cold 1 × PBS buffer (pH = 7.2). Cells were resuspended in 100 μL of cold 1 × PBS buffer and fixed with 70% aqueous ethanol overnight at 4 °C. DNA staining was done by resuspending the cell pellets in 1 × PBS solution containing PI (55 μg mL^{-1}) and RNaseA (100 μg mL^{-1}). Cell

https://dx.doi.org/10.1021/acs.inorgchem.0c00694
Inorg. Chem. XXXX, XXX, XXX−XXX

Scheme 1. Representative Synthetic Scheme of the Ligands (L1, L2) and Complexes 1−4

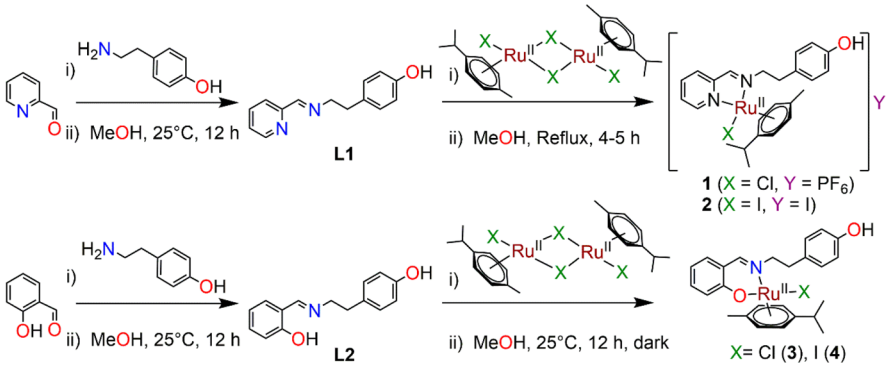

suspensions were gently mixed and incubated at 37 °C for 0.5 h. The samples were analyzed in a BD Biosciences FACS Calibur flow cytometer.

Determination of Intracellular Reactive Oxygen Species (ROS) Generation. A total of 5×10^4 MIA PaCa-2 cells were cultured in six-well plates. After 70% confluency, these cells were treated with **2** at two different concentrations (25 and 50 μM) for 6 h. After treatment, the medium, containing **2**, was removed. Cells were washed thoroughly two times with prewarmed (37 °C) 1 × PBS (pH = 7.2). The cells were then harvested by a quick trypsinization followed by washing with 1 × PBS. The cells were incubated with DCFH-DA solution (1 μM in 1 × PBS, pH = 7.2) in the dark for 15 min. Excess DCFH-DA was removed by centrifugation. A total of 500 μL of 1 × PBS was added to each well. Data were recorded and analyzed in a BD Biosciences FACS Calibur flow cytometer within 30 min of sample preparation.

Ruthenium Accumulation Study by ICP-MS. A total of 2×10^5 MIA PaCa-2 cells were seeded in 90 mm dia Petri dishes and incubated for 48 h. Equimolar concentrations (30 μM) of each complex were added, and incubation after drug treatment was allowed for a further 12 h. After removal of the medium, the cells were washed with PBS (pH = 7.4), treated with trypsin-EDTA, and counted and 1×10^6 cells were collected as cell pellets after centrifugation. Cell pellets were digested overnight in ICP-MS standard nitric acid (70% v/v) at 65 °C, followed by dilution with Milli-Q water to yield a final concentration of 4% HNO_3. The amount of Ru taken up by the cells was determined by a Thermo Scientific iCAP RQ ICP-MS of ThermoScientific. Analysis of each sample was carried out in triplicate, and the corresponding standard deviations were calculated. The standard ruthenium solutions were freshly prepared to generate the calibration curve.

Determination of Apoptosis by Annexin-V-PE/7-AAD Assay. Apoptosis was detected by PE-Annexin V/7-AAD dual staining apoptosis kit (BD Pharmingen, catalog no. 559763) by means of flow cytometry, as per the manufacturer's protocol. A total of 1×10^5 MIA PaCa-2 cells were seeded in 100 mm sterile tissue culture Petri dishes using 6 mL of DMEM medium. Then, the cells were incubated at 37 °C in a 5% CO_2 atmosphere for 48 h. After incubation, medium was changed and treated with two different concentrations of **2** (20 and 35 μM) for a 16 h period. The treated and untreated cells were harvested by cold 1 × PBS containing 0.1 mM EDTA and, subsequently, washed twice with cold 1 × PBS. Cells were resuspended in Annexin V binding buffer. Annexin V and 7-AAD were incubated for 15 min in the dark at 25 °C. Data were recorded and analyzed in a BD Biosciences FACSCalibur flow cytometer within 30 min of sample preparation.

Change in Mitochondrial Membrane Potential. Change in mitochondrial membrane potential (MMP, $\Delta\Psi_m$) was determined by flow cytometry after staining live MIA PaCa-2 cells with JC-1. A total of 1×10^5 MIA PaCa-2 cells were seeded in 100 mm sterile tissue culture Petri dishes. Then, the cells were incubated at 37 °C in a 5% CO_2 atmosphere for 48 h. After incubation, medium was changed and treated with two different concentrations of **2** (20 and 35 μM) for a 16 h period. Cells were harvested after removing the medium and washed with 1 × PBS. After the cells were washed twice with 1 × PBS, they were further resuspended in 1 × PBS, supplemented with 10% FBS. The solution was then incubated with 5 μg mL^{-1} of JC-1 for 15 min in the dark. After removal of supernatant, cells were suspended in 1 × PBS. Data were recorded and analyzed in a BD Biosciences FACSCalibur flow cytometer, measuring the red and green fluorescence intensities.

*Detection of ERK1/2 Phosphorylation in MIA-PaCa-2 Cells Following Treatment with Complexes **2** and **3**.* Cells were cultured on 100 mm dishes to 70% confluency and treated with 25 μM of **2** for 6 h. Cell pellets (both control and treated) washed with phosphate buffered saline (pH = 7.3) were suspended in 200 μL of RIPA lysis buffer. The resuspension was incubated on ice for 1 h with occasional mixing. The cell suspension was homogenized with a Dounce homogenizer with tight pestle (220 strokes). The resultant homogenate was centrifuged at 600*g* for 10 min followed by collection of the supernatant. The total protein in the lysate was estimated by Bradford (Sigma-Aldrich) assay. A total of 60 μg (control and treated) of lysate was mixed with gel loading dye (2% SDS, 2.5% β mercapto-ethanol, 7.5% glycerol, 2 M urea, and 0.005% bromophennol blue). The mixture was heated for 10 min at 95 °C then brought to room temperature, resolved in 12% denaturing polyacrylamide gel and transferred to a nitrocellulose membrane (BioRad Laboratories) at 180 mA current for 90 min. The membrane was blocked with 3% BSA (Sisco Research Laboratories) in TBS (Tris buffered saline) at room temperature for 2 h and incubated overnight at 4 °C with primary antibody [p44/42 MAPK (Erk1/2; Cell Signaling Technologies) and phospho-p44/42 MAPK (Thr202/Tyr204; Cell Signaling Technologies) 1:3300] in 1% BSA and 0.1% tween-20. The membrane was washed thrice with TBS (pH7.5) and thrice with TBS containing 0.1% Tween-20 (TBS-T). The resultant membrane was then incubated in goat anti-rabbit HRP conjugated secondary antibody (Santa Cruz Biotechnology) for 2 h at room temperature followed by washing in TBS-T (thrice) and in TBS (thrice). The chemiluminescence (clarity max, Biorad) was detected using a ChemiDoc Imaging System (170-01401; Bio-Rad) instrument.

RESULTS AND DISCUSSIONS

The tyramine based *N,N* and *N,O* chelating ligands (L1 and L2, respectively) were synthesized by modification of the reported literature procedures.[56,61] The ligands were prepared in a single step by condensing the respective aldehydes with the amines in methanol at room temperature for 12 h (Scheme 1). The complexes **1** and **2** were obtained by refluxing L1 with $[Ru^{II}(\eta^6\text{-}p\text{-cymene})X_2]_2$(X = Cl,I) in methanol for 4−5 h. Complexes **3** and **4** were synthesized by first deprotonating L2 with KOH, followed by stirring with $[Ru^{II}(\eta^6\text{-}p\text{-cymene})X_2]_2$(X = Cl, I) in methanol at room temperature for 12 h (Scheme 1). Complexes **3** and **4** required purification by column chromatography in neutral alumina, with 0.1% MeOH in DCM as an eluent. All four complexes were well-characterized by ^{1}H NMR, ^{13}C NMR, ESI-HRMS, UV−vis (Figure S16), and FT-IR (Figure S17). Complex **4** starts hydrolyzing into its corresponding aquated species within 2.5 h of ^{1}H NMR sample preparation in DMSO-d_6 due to the presence of residual water. Therefore, ^{13}C signals

https://dx.doi.org/10.1021/acs.inorgchem.0c00694
Inorg. Chem. XXXX, XXX, XXX−XXX

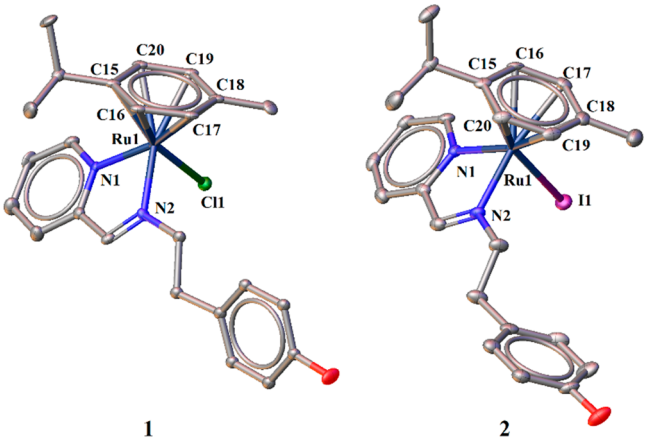

Figure 2. ORTEP diagrams of the complexes **1** and **2** with thermal ellipsoids at 50% probability level. The hydrogen atoms and counter-anions are omitted for clarity.

corresponding to the hydrolyzed complex appeared in the ^{13}C NMR spectrum after 2.5 h of acquisition. The bulk purity of the complexes was confirmed by elemental analyses. All four complexes exhibited UV peaks in the ranges 222−286 nm and 350−393 nm corresponding to the $\pi-\pi^*$ transitions, and the MLCT transitions appeared as a shoulder in the range 406−487 nm (Figure S16). The high resolution electrospray mass spectrometry confirmed the presence of the respective monocationic molecular ion peaks of **1**−**4**.

X-ray Crystallography. Good quality single crystals were obtained by layering acetonitrile solutions of the isolated complexes (**1** and **2**) with diethyl ether. The ORTEP diagrams of the complexes **1** and **2** are depicted in Figure 2. Complex **1** crystallized in the orthorhombic space group $P2_12_12_1$ (Table 1), while complex **2** in the monoclinic space group $P2_1/c$ (Table 1). In each complex, the metal center forms a tetrahedral structure where one vertex is occupied by a chloride/iodide, two vertices by the donor atoms of the ligand (*N*,*N* of L1), and the fourth vertex by the *p*-cymene moiety with a η^6 mode of bonding. The ^1H NMR spectrum shows that the two methyl groups of the isopropyl moiety in *p*-cymene are no longer equivalent after formation of the complexes. This is also supported by the bond parameters in Table 2. The lattice PF_6^- or the I^- group balances the resultant mono-positive charge on the metal center in **1** and **2**, respectively.

Stability in Aqueous Buffer Solution. The hydrolysis of complexes **1**−**4** was studied in a 3:7 (v/v) DMSO-d_6/10 mM PBS buffer (pD = 7.4) containing 4 mM NaCl by ^1H NMR. In the case of **1**, ^1H peaks corresponding to gradual formation of the aquated complex and a significant amount of dissociation started after 6 h in ^1H NMR (Supporting Information, Figure

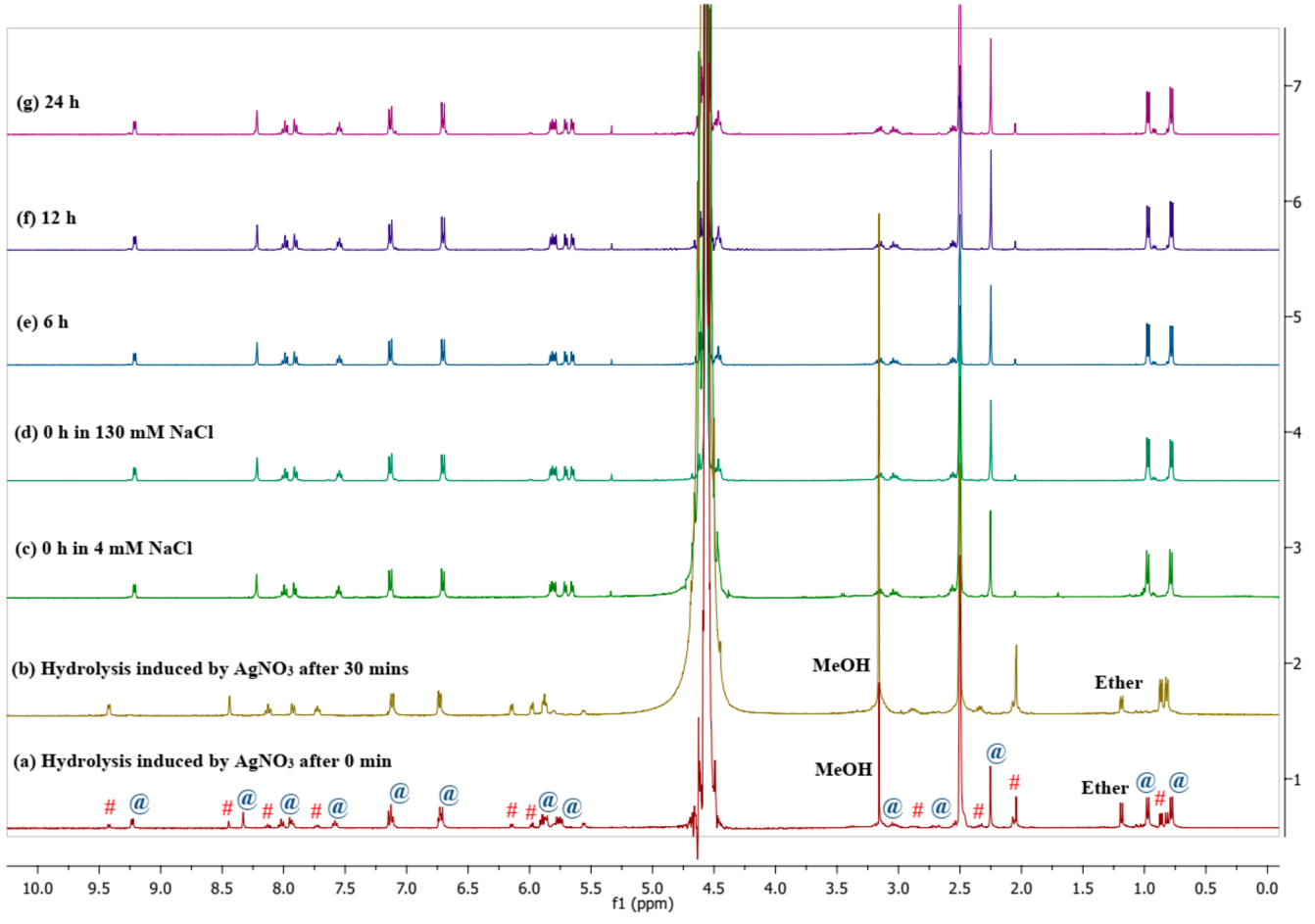

Figure 3. A stack plot of $AgNO_3$ induced hydrolysis of complex **2** in 3:7 (v/v) DMSO-d_6/D_2O (containing 1.1 equiv of $AgNO_3$; a,b) correlated with spectra acquired in the presence of 3:7 (v/v) DMSO-d_6/10 mM phosphate buffered solution (pD = 7.4) with (c) 4 and (d−g) 130 mM NaCl at different time intervals. "#" stands for hydrolyzed peaks induced by $AgNO_3$, while "@" represents peaks of intact **2**.

https://dx.doi.org/10.1021/acs.inorgchem.0c00694
Inorg. Chem. XXXX, XXX, XXX−XXX

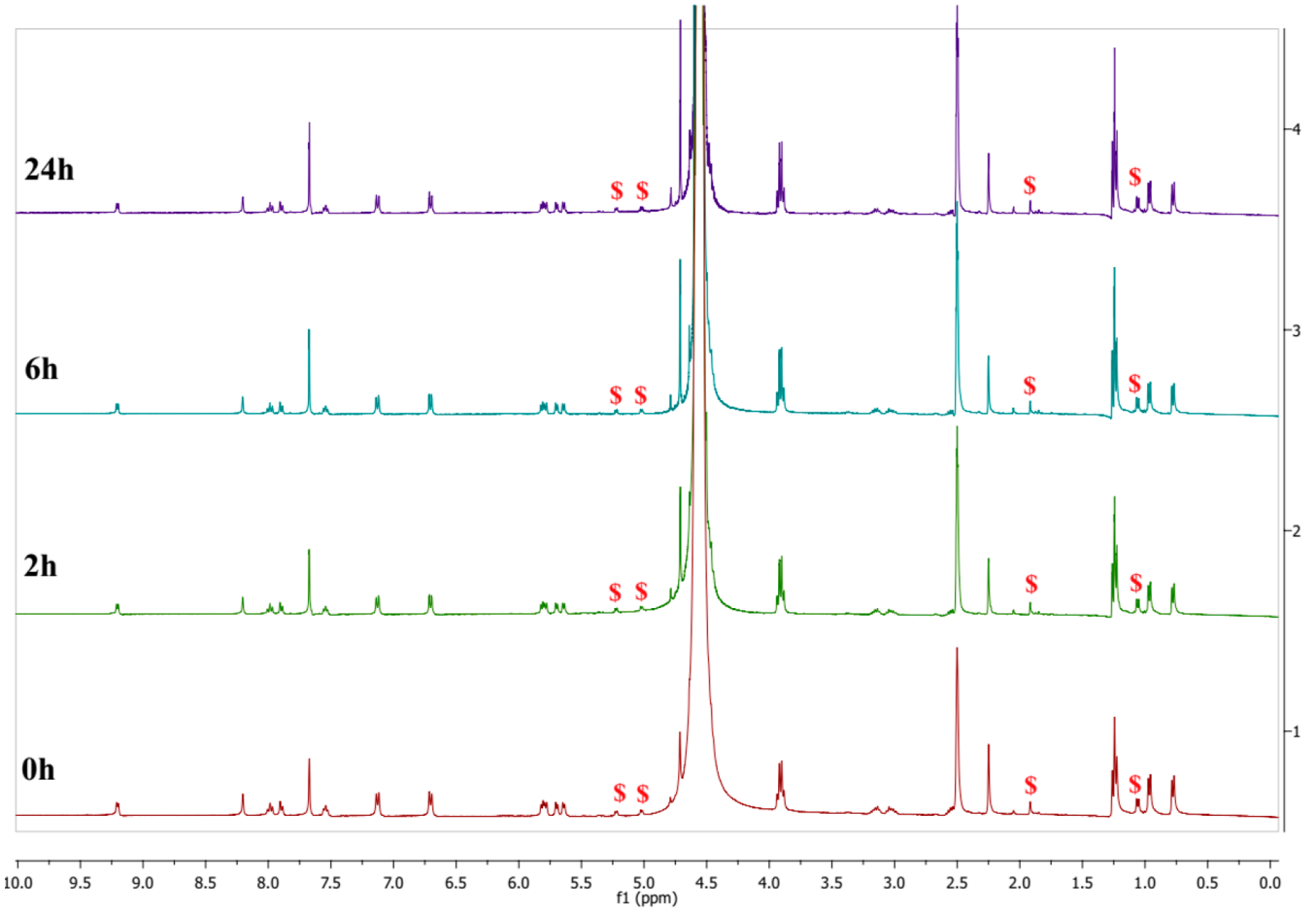

Figure 4. A stack plot of the ^{1}H NMR spectrum to study 9-EtG binding of complex **2** in 3:7 (v/v) DMSO-d_6/10 mM phosphate buffer solution (pD = 7.4) containing 4 mM NaCl and 2 equiv of 9-EtG. "$" represents ruthenium(II) hydroxo dimer of formulation $[Ru_2(p\text{-cym})_2(OH)_3]^+$.

S18). The ESI-HRMS of **1**, displayed hydrolyzed and dissociated peaks, after incubation for 14 h (Supporting Information, Figures S19 and S20), showing relatively poor stability. Complex **2** bearing the Ru−I bond did not show any aquation, and exchange of the halide (4 mM or 130 mM NaCl, 10 mM PBS buffer, pD = 7.4) did not take place in the 24 h observation period. Thus, complex **2** is highly stable in the aqueous buffer (Figure 3). A stack plot of **1** (4 mM NaCl, pD = 7.4) compared with that of **2** (130 mM NaCl) showed a difference in peak positions and multiplicities, especially in the *p*-cymene region (Figure S22). $AgNO_3$ induced hydrolysis of **2** resulted in complete conversion to the corresponding aquated species within 30 min. The relevant ^{1}H signals shifted to higher parts per million supporting aquation (Figure 3). The above results suggest that **2** is inert toward exchange of the iodide ligand with chloride or water. ESI-HRMS also confirmed the inertness of **2** toward chloride exchange even at micromolar concentrations. In the presence of 2:8 v/v methanol/10 mM PBS buffer (pH = 7.4) containing 130 mM NaCl, only a minute amount of the molecular ion peak of **1** ($[Ru(L1)(p\text{-cymene})\text{-}Cl]^+$) corresponding to m/z of 497.0928 (calcd 497.0903) was observed after the incubation period of 14 h (Supporting Information, Figures S23 and S24).

In addition, complexes **1** and **2** were also studied in 1:9 (v/v) methanol/PBS buffer with 4 mM NaCl at pH = 7.4 for their stability using UV−visible spectroscopy. Even at such a lower concentration of 10^{-5} M, the complexes show similar behavior to that found from the NMR and ESI-MS studies. Complex **1** hydrolyzes, but complex **2** stays intact even after 24 h (Figure S25).

On the contrary, the monoaquated species of **3** and **4** were formed almost instantaneously under the same buffer conditions. We observed peaks corresponding to the hydrolyzed species from the beginning. This was corroborated in a 3:7 (v/v) DMSO-d_6/D_2O mixture, containing 1.5 equiv of $AgNO_3$, to induce precipitation of the respective halides. The ^{1}H NMR corresponded exactly with the spectra obtained in absence of $AgNO_3$, as no chemical shift was observed. The hydrolyzed complexes remain stable up to 24 h (Supporting Information, Figures S26, S27). Our earlier results[64] with these types of complexes and similar examples in literature[65] suggest that perhaps the resultant monocationic Ru^{II} is the more preferred state.

Binding Studies with Model Nucleobase 9-Ethylguanine (9-EtG) and L-Glutathione (GSH). The ^{1}H NMR of **2** also does not show any peaks corresponding to any 9-EtG adduct (Figure 4). However, the ^{1}H NMR showed a small amount of the Ru^{II} hydroxo dimer of formulation $[Ru_2(p\text{-cym})_2(OH)_3]^+$ with ^{1}H signals at 5.1 and 5.4 ppm (Figure 4).[52,66] Complexes **1** and **2** did not exhibit any adduct with 5 equiv of 9-EtG when investigated by ESI-HRMS up to 24 and 72 h, respectively (Supporting Information, Figures S28, S29, S30),

https://dx.doi.org/10.1021/acs.inorgchem.0c00694
Inorg. Chem. XXXX, XXX, XXX−XXX

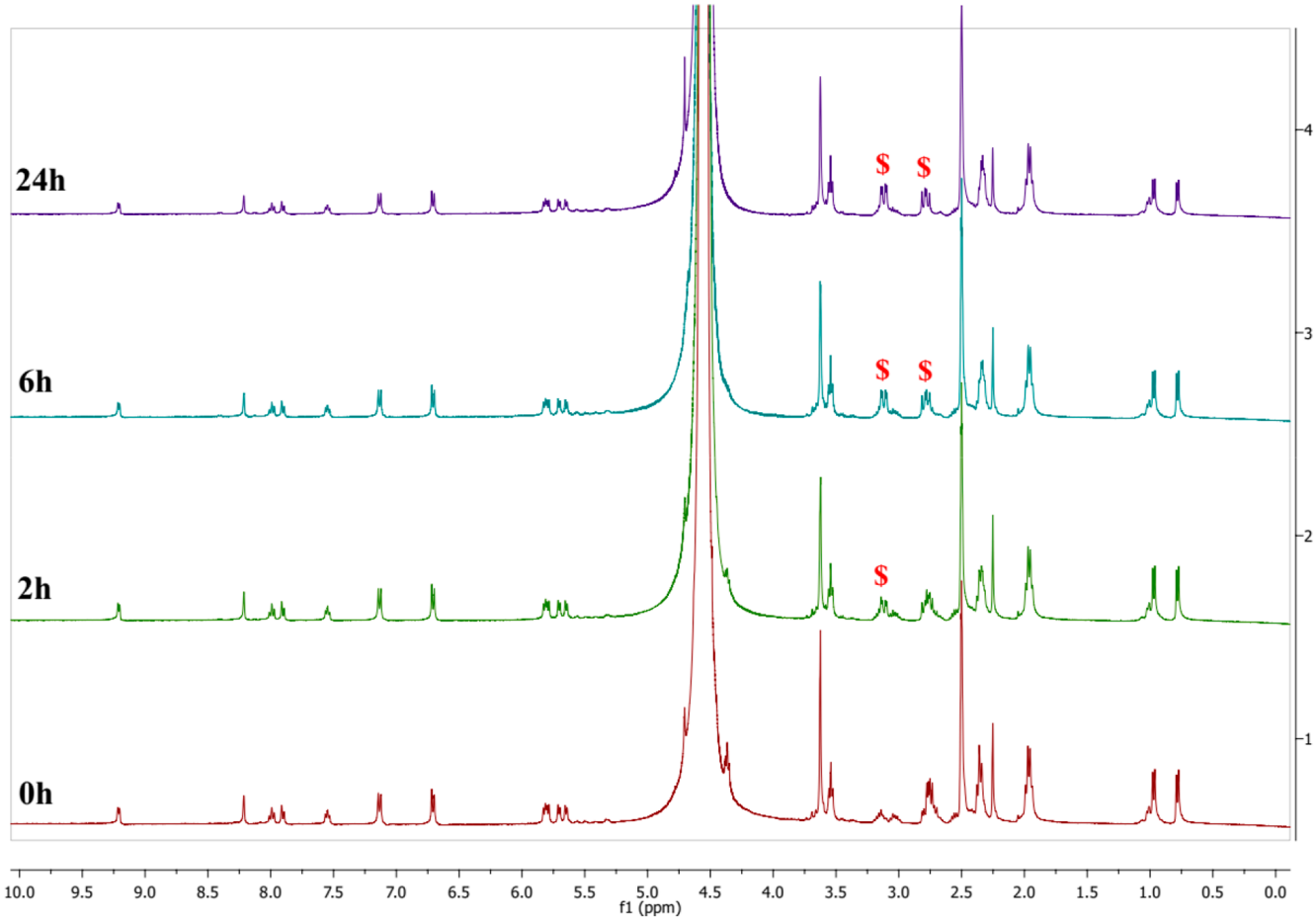

Figure 5. A stack plot of ^{1}H NMR spectrum to study GSH binding of complex **2** in 3:7 (v/v) DMSO-d_6/10 mM phosphate buffer solution (pD = 7.4) containing 4 mM NaCl and 2 equiv of reduced L-glutathione (GSH). "$" represents glutathione auto-oxidation peaks.

using concentrations as low as 20−30 μM during incubation. We also performed the 9-EtG binding study for **2** in ESI-MS by hydrolyzing the complex with a stoichiometric amount (0.5 equiv) of $AgNO_3$ and then adding 9-EtG followed by incubation at 37 °C. We found the 9-EtG adduct of **2** formed within 30 min. Thus, if inside the cell the iodide group is lost, then **2** may bind to DNA. The 9-EtG bound adducts of **3** and **4** (m/z 655.1962 and 655.2018, respectively) were observed only after 72 h of incubation in ESI-HRMS (Supporting Information, Figures S31, S32). In spite of the halide being released almost instantaneously from **3** and **4** (Supporting Information, Figures S26, S27), the above data suggest that **3** and **4** bind to the N^7 of 9-EtG but are less reactive toward such adduct formation.

In the case of **1**, upon incubation with GSH, the hydrolysis was suppressed as evident from ^{1}H NMR, and a minute amount of the GSH bound **1** started to appear within 12 h (Supporting Information, Figure S33). ESI-HRMS, indicated the formation of the GSH bound adduct of **1** (m/z: 768.2024), within 3 h of sample preparation, which gradually increased in intensity over 24 h (Supporting Information, Figures S34, S35). The lower concentration of **2** in ESI-MS studies may be responsible for driving the GSH adduct formation. Complex **2** did not show any adduct with reduced L-glutathione (GSH; 2 equiv with respect to **2**) in the presence of 3:7 (v/v) DMSO-d_6/10 mM PBS buffer (pD = 7.4) containing 4 mM NaCl by ^{1}H NMR up to 24 h. The peaks due to the auto oxidation of GSH leading to GSSG started to appear after 2 h (Figure 5). The ^{1}H NMR data were supported by the ESI-HRMS study where a micromolar concentration of **2** was incubated with 5 equiv of L-glutathione in the presence of 2:8 v/v methanol/10 mM PBS buffer (pH = 7.4) containing 4 mM NaCl. Even under this condition, no binding with GSH was observed until 24 h. The molecular ion peak at m/z 589.0228 remained intact (Supporting Information, Figures S36, S37). Complexes **3** and **4** almost completely degraded to multiple species in the presence of 5 equiv of GSH as observed in ESI-HRMS within 12 h (Supporting Information, Figures S38−S41).

Distribution Coefficient Determination. The cellular uptake and cytotoxic efficacy of Ru^{II} (p-cymene) complexes are correlated with their lipophilic behavior. The distribution coefficient (log D) values of complexes **1**−**4** were determined in an octanol/PBS buffer system. The log D values are 0.26 ± 0.01, 1.44 ± 0.08, and 2.17 ± 0.2 for **2**, **3**, and **4**, respectively, well within the range of Lipinski's Rule of 5.0, which are the conditions required for a good drug candidate. Complex **1** is the most hydrophilic in the family, displaying a log D value of −0.49 ± 0.02 (Figure 6). The aqueous layer of **1** was also investigated for speciation by ESI-HRMS. The spectra matched well with **1** recorded in the presence of 2:8 v/v methanol/10 mM PBS buffer (pH = 7.4) containing 4 mM NaCl (Figure S20) after incubation for 14 h showing that the quick aquation and

https://dx.doi.org/10.1021/acs.inorgchem.0c00694
Inorg. Chem. XXXX, XXX, XXX−XXX

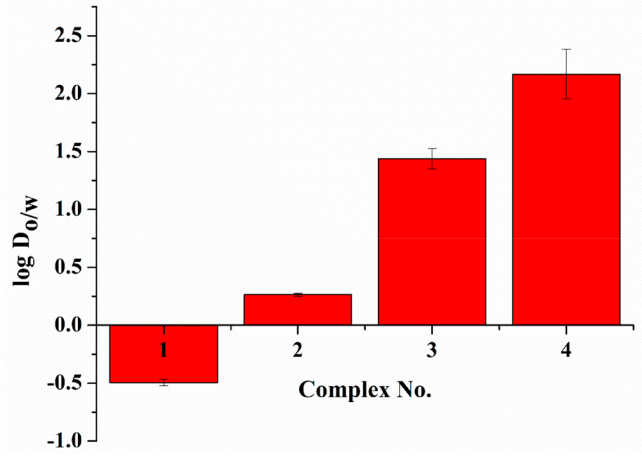

Figure 6. Lipophilicity of the complexes (**1**−**4**) in a 1:1 (v/v) octanol/PBS buffer mixture at 37 °C.

subsequent speciation is responsible for the higher hydrophilicity of **1** (Figure S21).

In Vitro Cytotoxicity. The synthesized complexes were investigated for their *in vitro* toxicity against MDA-MB-231 (triple-negative breast adenocarcinoma), Hep G2 (hepatocellular carcinoma), MIA PaCa-2 (pancreas ductal adenocarcinoma), and HFF-1 (human normal foreskin fibroblasts). The activities are tabulated in the form of the corresponding IC_{50} values in Table 3.

Table 3. IC_{50}(μM) ± SD Values[a] of Complexes 1−4 against a Panel of Carcinoma Cell Lines and HFF-1 (SD = Standard Deviation)

complexes	MDA-MB-231	Hep G2	MIA PaCa-2	HFF-1
1	>50	>100	>50	>100
2	>50	>75	5 ± 1	>100
3	42 ± 3	58 ± 5	56 ± 2	54 ± 3
4	44 ± 4	57 ± 4	60 ± 3	57 ± 2

[a]Complexes were treated for 72 h. IC_{50} values were calculated by nonlinear curve fitting in dose response inhibition-variable slope model using graph pad prism. The data presented are means of three independent experiments; in a single experiment each concentration was assayed in triplicate. The statistical significance (p) of the data is <0.05 or better.

Compounds **3** and **4** exhibited more or less comparable IC_{50} values in the three tested carcinoma cell lines, as well as in HFF-1 (Supporting Information, Figures S42, S43). Complex **2** displayed a time dependent increase in cytotoxicity against MIA PaCa-2 with the IC_{50} improving from ca. 35 μM (48 h incubation with **2**) to 5 μM (72 h incubation with **2**; Supporting Information, Figure S44), while maintaining a value of >50 μM in MDA-MB-231, >75 μM in Hep-G2, and >150 μM in HFF-1. It is worth mentioning here that MIA PaCa-2 is an aggressive pancreatic cell line with high tumorigenicity.[67]

Specificity is a prime focus in this field of study, and such a behavior in Ru^{II} complexes is scarce in the literature. Ru^{II} complexes which are strongly resistant toward hydrolysis and yet display potent cytotoxic activities (based upon the behavior of **2**), are quite numerous in the literature.[68−71] Our earlier work has shown a cytotoxic imidazole-based Ru^{II} (*p*-cymene) complex with resistance toward hydrolysis and efflux from cells through ATP7B and was significantly cytotoxic (IC_{50} = 6−14 μM) to cells.[72] Sadler et al. reported Ru^{II} complexes with redox-active diamine ligands with variation in arenes. Among them, certain *p*-cymene and bipyridine based Ru^{II} complexes exhibited selective cytotoxicity toward A2780, while being inactive against A549.[73] Certain tetranuclear Ru^{II} (*p*-cymene) complexes were toxic against A2780 and cisplatin-resistant A2780, but did not show any activity against lung NCI-H460.[74] Two *p*-cymene based acylpyrazolonato based Ru^{II} complexes showed specific activity against Hep-G2 among a panel of four cancer cell lines (no nontumorogenic cell line was investigated).[75] The studies above did not show any result of cytotoxicity on primary cell lines. In all the above literature, as well as the current work presented here, it was not possible to understand the exact reason of specificity. A Ru^{II} metallacycle with bromide as a counteranion and a series of Ru^{II} (*p*-cymene) based complexes bearing 1,2,3,4-tetrahydroisoquinoline amino alcohol ligands have shown specific toxicity toward a particular cell line while being inactive against normal cells.[76,77] Herein, we showcase a *p*-cymene based Ru^{II} complex which is effective against a particular form of pancreatic carcinoma (MIA PaCa-2) but not cytotoxic to normal fibroblasts (HFF-1) or other investigated cancer cells. Hence, among the four Ru^{II} complexes, **2** may act as a model complex to start investigation around the ligand environment and measure the effect on cells. The complex shows the change in activity keeping the same ligand and metal center but just by changing the coordinated halide. The effect of the change in the coordinated halide is so pronounced that the iodido coordinated **2** is stable toward hydrolysis and does not react with GSH in the 24 h period of study. However, **1** shows quick aquation and the initiation of dissociation within 6 h. The change of the coordination motif from *N,N* to *N,O* altered the cytotoxicity pattern, and the complexes are toxic to all cells, with a greater dose requirement.

The ESI-HRMS results suggest that DNA is a possible target for complex **2** only upon the loss of the coordinated iodide since it reacts with 9-EtG only under such conditions. The increase in the cytotoxicity of **2** with time suggests that slow dissociation may be responsible for its better activity upon longer incubation periods. The best complex in the series, **2**, is unique since many Ru^{II} (*p*-cymene) complexes have been reported to be toxic to pancreatic carcinomas, namely, BxPC-3,[78] PANC-1,[42] DAN-G,[79,80] CAPAN-1,[81] and MIA PaCa-2,[82−86] but none of them are selective.

Ruthenium Accumulation Study by ICP-MS. The ICP-MS data in MIA PaCa-2 cells with the Ru^{II} complexes (**1**−**4**) showed that ruthenium accumulation for **2** was highest when incubated with equimolar concentrations of each complex (**1**−**4**) for 12 h. The order of accumulation is **2** > **3** > **1** > **4** (Figure 7). Thus, the internalization studies suggest that **2** should be more active than **1**, **3**, and **4**, which matches well with the cytotoxicity data. Among **1** and **4**, **1** is internalized more but still the toxicity of **4** is higher. This is well correlated with the higher stability of **4** compared to **1**. Both of them form aquated species, which is stable in **4** for 24 h, whereas it starts to dissociate further in the case of **1** after 6 h.

Investigation of Apoptosis. Annexin V-PE/7-AAD double staining assay using two different dosages (20 and 35 μM) of **2** showed that there is 31% and 42% apoptosis, respectively, compared to 0.9% in the control (Figures 8, S45). Thus, with an increase in dose, the percentage of apoptosis also increases (Supporting Information, Figure S45). Investigation of accumulation of reactive oxygen species (ROS) in the cytotoxicity of **2** showed that there is no significant difference

https://dx.doi.org/10.1021/acs.inorgchem.0c00694
Inorg. Chem. XXXX, XXX, XXX−XXX

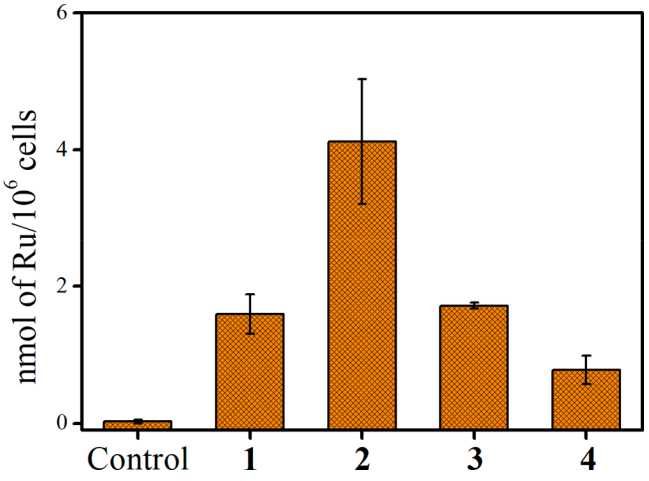

Figure 7. ICP-MS study depicting the internalization of complexes **1**−**4** in MIA PaCa-2 cells. Each data point is the mean of three independent experiments.

in the accumulation of ROS compared to the control using two different dosages of **2** (25 and 50 μM) against MIA PaCa-2, using DCFH-DA assay through flow cytometry (Figure 8). Hence, it is ascertained that ROS is not involved. The result is not completely unexpected since, in ROS based cell killing, the other cancer cells should also be affected, unlike that observed for **2**, which shows specificity toward MIA PaCa-2. In addition, we studied the ERK1/2 (extracellular signal regulated kinase) phosphorylation downstream of MAPK (mitogen-activated protein kinase) for the MIA PaCa-2 selective complex **2**. The MAPK may be activated by different pathways including oxidative stress.[87,88] There was no change in the level of ERK1/2 phosphorylation in the cells treated with a 25 μM concentration of **2** for 6 h (Figure S46). Thus no increase in the ROS content or the phosphorylation of ERK1/2 suggests that complex **2** is not acting through the oxidative stress pathway.

A flow cytometric investigation of complex **2** for its effect on the cell cycle in MIA PaCa-2 shows an arrest in the G_0/G_1 phase (Figures 8, S47). In the G_1 phase, the cells synthesize various mRNA's and proteins for proper replication of DNA in the S phase.[89] Hence, complex **2** may be inhibiting the biosynthetic process which consequently hindered the cell cycle progression to the S phase. Complex **2** showed depolarization of mitochondria further supporting apoptosis. The JC-1 dye exhibits a red emission (λ_{em} = 590 nm) in aggregated state when the mitochondrial potential is intact. Once the mitochondrial membrane potential is compromised, JC-1 remains as a monomer, emitting green fluorescence (λ_{em} = 550 nm).[90] MIA PaCa-2 cells treated with two different dosages of **2** (20 and 35 μM) for 16 h exhibited an increase in the green fluorescence intensity from 1.5% in control to 7% and 9.5%, respectively, in a dose-dependent manner (Figures 8, S48). The mitochondrial depolarization by **2** supports the apoptotic

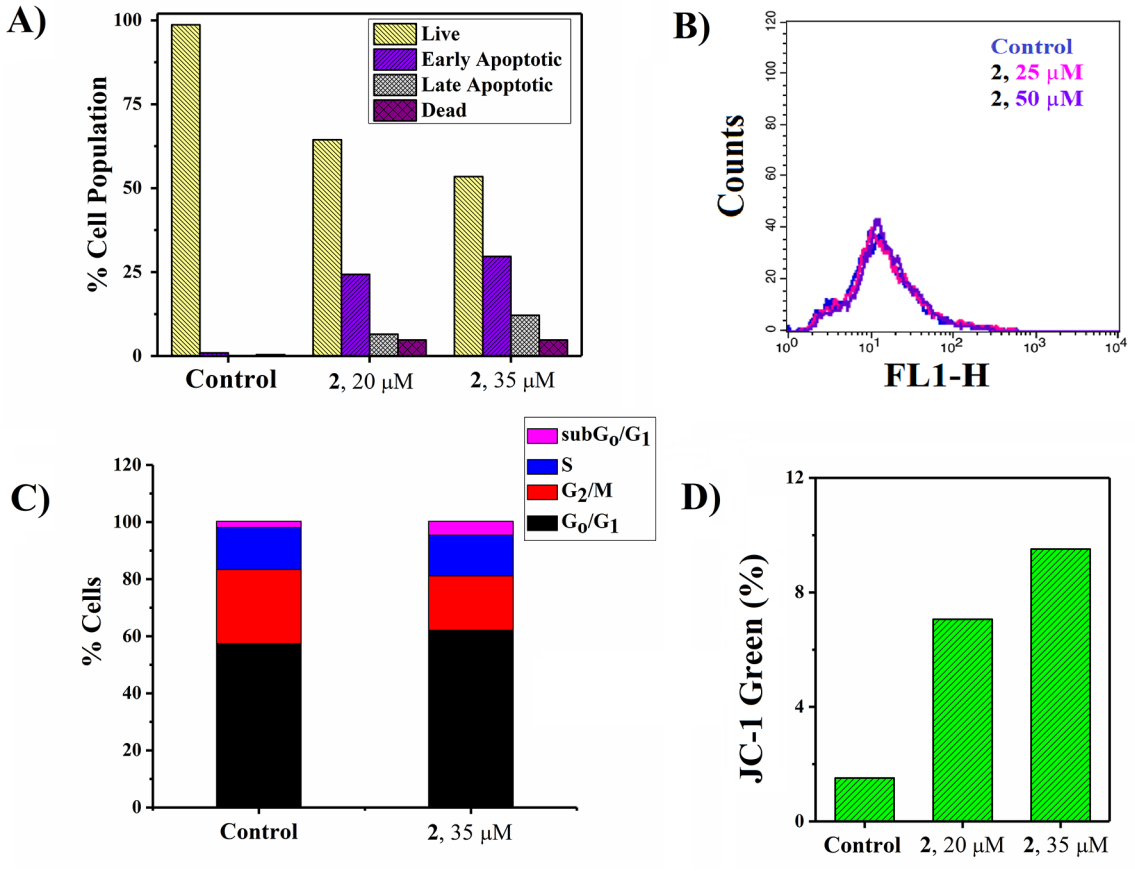

Figure 8. *In vitro* mechanistic studies of complex **2** against MIA PaCa-2 using flow cytometry. (A) Induction of apoptosis by 20 and 35 μM in a dose-dependent manner. (B) Investigation of total reactive oxygen species (ROS) generation using DCFH-DA with 25 and 50 μM. (C) Cell cycle analysis against MIA PaCa-2 with 35 μM concentration. (D) Mitochondrial membrane depolarization induced by 20 and 35 μM in a dose-dependent manner using JC-1 (5 μg/mL).

https://dx.doi.org/10.1021/acs.inorgchem.0c00694
Inorg. Chem. XXXX, XXX, XXX−XXX

pathway, but the depolarization is not significant enough to conclude if the intrinsic pathway is the major pathway of apoptosis.

CONCLUSIONS

The Ru^{II} (*p*-cymene) complex (**2**) with a *N*,*N* coordination and iodido linkage showed specific cytotoxicity against the pancreatic carcinoma, MIA PaCa-2, while being inactive against normal human foreskin fibroblasts (HFF-1). Complex **2** displayed excellent stability in aqueous buffer solution (pH = 7.4) and is strongly resistant toward chloride exchange or binding toward GSH. In contrast, the chloro analogue **1** undergoes quick aquation and then, after 6 h, starts to dissociate. The chloro analogue is also not appreciably cytotoxic. Complexes **1** and **2** do not interact with 9-EtG, but **3** and **4** show weak interaction with 9-EtG after 72 h. The *N*,*O* coordinated Ru^{II} (*p*-cymene) complexes display immediate aquation by releasing the coordinated halide and bind to GSH, leading to almost complete degradation in 14 h. The cellular uptake of complex **2** in MIA PaCa-2 is highest compared to the other three complexes. Complex **2** depolarizes the mitochondria and induces cell killing via apoptosis.

ASSOCIATED CONTENT

Supporting Information

The Supporting Information is available free of charge at https://pubs.acs.org/doi/10.1021/acs.inorgchem.0c00694.

^{1}H NMR and ^{13}C NMR of ligands (L1, L2; Figures S1−S4) and complexes (**1**−**4**; Figures S5−S15), UV−visible and FT-IR spectra of complexes **1**−**4** (Figures S16 and S17), hydrolysis kinetics of complexes **1**−**4** by ^{1}H NMR and ESI-HRMS (Figures S18−S27), 9-EtG binding kinetics of complexes **1**−**4** by ^{1}H NMR and ESI-HRMS (Figures S28−S32), GSH binding kinetics of complexes **1**−**4** by ^{1}H NMR and ESI-HRMS (Figures S33−S41), MTT assay plots (Figures S42−S44), various pathways of cell killing by complex **2**, e.g., apoptosis and mitochondrial membrane depolarization (Figures S45−S48) (PDF)

Accession Codes

CCDC 1969294−1969295 contain the supplementary crystallographic data for this paper. These data can be obtained free of charge via www.ccdc.cam.ac.uk/data_request/cif, or by emailing data_request@ccdc.cam.ac.uk, or by contacting The Cambridge Crystallographic Data Centre, 12 Union Road, Cambridge CB2 1EZ, UK; fax: +44 1223 336033.

AUTHOR INFORMATION

Corresponding Author

Arindam Mukherjee − *Department of Chemical Sciences and Centre for Advanced Functional Materials (CAFM), Indian Institute of Science Education and Research Kolkata, Mohanpur Campus, Mohanpur 741246, India*; orcid.org/0000-0001-9545-8628; Email: a.mukherjee@iiserkol.ac.in

Authors

Arpan Mukherjee − *Department of Chemical Sciences and Centre for Advanced Functional Materials (CAFM), Indian Institute of Science Education and Research Kolkata, Mohanpur Campus, Mohanpur 741246, India*

Sourav Acharya − *Department of Chemical Sciences and Centre for Advanced Functional Materials (CAFM), Indian Institute of Science Education and Research Kolkata, Mohanpur Campus, Mohanpur 741246, India*; orcid.org/0000-0001-5511-1312

Kallol Purkait − *Department of Chemical Sciences and Centre for Advanced Functional Materials (CAFM), Indian Institute of Science Education and Research Kolkata, Mohanpur Campus, Mohanpur 741246, India*

Kaustav Chakraborty − *Amity Institute of Biotechnology, Amity University Kolkata, Newtown, Kolkata 700135, India*

Ashima Bhattacharjee − *Amity Institute of Biotechnology, Amity University Kolkata, Newtown, Kolkata 700135, India*

Complete contact information is available at: https://pubs.acs.org/10.1021/acs.inorgchem.0c00694

Author Contributions

[§]These authors contributed equally.

Notes

The authors declare no competing financial interest.

ACKNOWLEDGMENTS

The authors sincerely thank SERB for funding via EMR/2017/002324. The authors also thank IISER Kolkata for infrastructural and financial support. A.B. is sincerely thankful for the Ramanujan Fellowship Project (SB/S2/RJN-106/2015), SERB, DST. A.M. thanks CSIR. S.A. and K.P. thank U.G.C. for their research fellowships. The authors sincerely thank Mr. Tamal Ghosh for help in the flow cytometry studies. The authors also thank Dr. Keka Mukherjee (CGCRI, Kolkata) for help in elemental analysis.

REFERENCES

(1) Jemal, A.; Bray, F.; Center, M. M.; Ferlay, J.; Ward, E.; Forman, D. Global cancer statistics. *Ca-Cancer J. Clin.* **2011**, *61*, 69−90.

(2) Romero-Canelon, I.; Sadler, P. J. Next-Generation Metal Anticancer Complexes: Multitargeting via Redox Modulation. *Inorg. Chem.* **2013**, *52*, 12276−12291.

(3) Wang, X.; Wang, X.; Jin, S.; Muhammad, N.; Guo, Z. Stimuli-Responsive Therapeutic Metallodrugs. *Chem. Rev.* **2019**, *119*, 1138−1192.

(4) Kenny, R. G.; Marmion, C. J. Toward Multi-Targeted Platinum and Ruthenium Drugs-A New Paradigm in Cancer Drug Treatment Regimens? *Chem. Rev.* **2019**, *119*, 1058−1137.

(5) Meier-Menches, S. M.; Gerner, C.; Berger, W.; Hartinger, C. G.; Keppler, B. K. Structure-activity relationships for ruthenium and osmium anticancer agents - towards clinical development. *Chem. Soc. Rev.* **2018**, *47*, 909−928.

(6) Zhao, J.; Li, S.; Wang, X.; Xu, G.; Gou, S. Dinuclear Organoruthenium Complexes Exhibiting Antiproliferative Activity through DNA Damage and a Reactive-Oxygen-Species-Mediated Endoplasmic Reticulum Stress Pathway. *Inorg. Chem.* **2019**, *58*, 2208−2217.

(7) Zhang, C.; Guan, R.; Liao, X.; Ouyang, C.; Rees, T. W.; Liu, J.; Chen, Y.; Ji, L.; Chao, H. A mitochondria-targeting dinuclear Ir-Ru complex as a synergistic photoactivated chemotherapy and photodynamic therapy agent against cisplatin-resistant tumour cells. *Chem. Commun.* **2019**, *55*, 12547−12550.

(8) Wernitznig, D.; Kiakos, K.; Del Favero, G.; Harrer, N.; Machat, H.; Osswald, A.; Jakupec, M. A.; Wernitznig, A.; Sommergruber, W.; Keppler, B. K. First-in-class ruthenium anticancer drug (KP1339/IT-139) induces an immunogenic cell death signature in colorectal spheroids in vitro. *Metallomics* **2019**, *11*, 1044−1048.

(9) Mitrovic, A.; Kljun, J.; Sosic, I.; Ursic, M.; Meden, A.; Gobec, S.; Kos, J.; Turel, I. Organoruthenated Nitroxoline Derivatives Impair Tumor Cell Invasion through Inhibition of Cathepsin B Activity. *Inorg. Chem.* **2019**, *58*, 12334−12347.

(10) McCain, J.; Colon, K. L.; Barrett, P. C.; Monro, S. M. A.; Sainuddin, T.; Roque, J., III; Pinto, M.; Yin, H.; Cameron, C. G.; McFarland, S. A. Photophysical Properties and Photobiological Activities of Ruthenium(II) Complexes Bearing π-Expansive Cyclometalating Ligands with Thienyl Groups. *Inorg. Chem.* **2019**, *58*, 10778−10790.
(11) Liu, J.; Lai, H.; Xiong, Z.; Chen, B.; Chen, T. Functionalization and cancer-targeting design of ruthenium complexes for precise cancer therapy. *Chem. Commun.* **2019**, *55*, 9904−9914.
(12) Liu, C.; Zhang, R.; Zhang, W.; Liu, J.; Wang, Y.-L.; Du, Z.; Song, B.; Xu, Z. P.; Yuan, J. "Dual-Key-and-Lock" Ruthenium Complex Probe for Lysosomal Formaldehyde in Cancer Cells and Tumors. *J. Am. Chem. Soc.* **2019**, *141*, 8462−8472.
(13) Lin, Y.; Wang, J.; Zheng, W.; Luo, Q.; Wu, K.; Du, J.; Zhao, Y.; Wang, F. Organometallic ruthenium anticancer complexes inhibit human peroxiredoxin I activity by binding to and inducing oxidation of its catalytic cysteine residue. *Metallomics* **2019**, *11*, 546−555.
(14) Kladnik, J.; Kljun, J.; Burmeister, H.; Ott, I.; Romero-Canelon, I.; Turel, I. Towards Identification of Essential Structural Elements of Organoruthenium(II)-Pyrithionato Complexes for Anticancer Activity. *Chem. - Eur. J.* **2019**, *25*, 14169−14182.
(15) Corte-Real, L.; Karas, B.; Bras, A. R.; Pilon, A.; Avecilla, F.; Marques, F.; Preto, A.; Buckley, B. T.; Cooper, K. R.; Doherty, C.; Garcia, M. H.; Valente, A. Ruthenium-Cyclopentadienyl Bipyridine-Biotin Based Compounds: Synthesis and Biological Effect. *Inorg. Chem.* **2019**, *58*, 9135−9149.
(16) Ballester, F. J.; Ortega, E.; Porto, V.; Kostrhunova, H.; Davila-Ferreira, N.; Bautista, D.; Brabec, V.; Dominguez, F.; Santana, M. D.; Ruiz, J. New half-sandwich ruthenium(II) complexes as proteosynthesis inhibitors in cancer cells. *Chem. Commun.* **2019**, *55*, 1140−1143.
(17) Tian, Z.; Li, J.; Zhang, S.; Xu, Z.; Yang, Y.; Kong, D.; Zhang, H.; Ge, X.; Zhang, J.; Liu, Z. Lysosome-Targeted Chemotherapeutics: Half-Sandwich Ruthenium(II) Complexes That Are Selectively Toxic to Cancer Cells. *Inorg. Chem.* **2018**, *57*, 10498−10502.
(18) Thota, S.; Rodrigues, D. A.; Crans, D. C.; Barreiro, E. J. Ru(II) Compounds: Next-Generation Anticancer Metallotherapeutics? *J. Med. Chem.* **2018**, *61*, 5805−5821.
(19) Pettinari, R.; Marchetti, F.; Di Nicola, C.; Pettinari, C.; Galindo, A.; Petrelli, R.; Cappellacci, L.; Cuccioloni, M.; Bonfili, L.; Eleuteri, A. M.; Guedes da Silva, M. F. C.; Pombeiro, A. J. L. Ligand Design for N, O- or N, N-Pyrazolone-Based Hydrazones Ruthenium(II)-Arene Complexes and Investigation of Their Anticancer Activity. *Inorg. Chem.* **2018**, *57*, 14123−14133.
(20) Martinez-Pena, F.; Infante-Tadeo, S.; Habtemariam, A.; Pizarro, A. M. Reversible pH-Responsive Behavior of Ruthenium(II) Arene Complexes with Tethered Carboxylate. *Inorg. Chem.* **2018**, *57*, 5657−5668.
(21) Li, J.; Tian, M.; Tian, Z.; Zhang, S.; Yan, C.; Shao, C.; Liu, Z. Half-Sandwich Iridium(III) and Ruthenium(II) Complexes Containing P-P-Chelating Ligands: A New Class of Potent Anticancer Agents with Unusual Redox Features. *Inorg. Chem.* **2018**, *57*, 1705−1716.
(22) Li, J.; Guo, L.; Tian, Z.; Zhang, S.; Xu, Z.; Han, Y.; Li, R.; Li, Y.; Liu, Z. Half-Sandwich Iridium and Ruthenium Complexes: Effective Tracking in Cells and Anticancer Studies. *Inorg. Chem.* **2018**, *57*, 13552−13563.
(23) Lam, N. Y. S.; Truong, D.; Burmeister, H.; Babak, M. V.; Holtkamp, H. U.; Movassaghi, S.; Ayine-Tora, D. M.; Zafar, A.; Kubanik, M.; Oehninger, L.; Sohnel, T.; Reynisson, J.; Jamieson, S. M. F.; Gaiddon, C.; Ott, I.; Hartinger, C. G. From Catalysis to Cancer: Toward Structure-Activity Relationships for Benzimidazol-2-ylidene-Derived N-Heterocyclic-Carbene Complexes as Anticancer Agents. *Inorg. Chem.* **2018**, *57*, 14427−14434.
(24) Haghdoost, M. M.; Guard, J.; Golbaghi, G.; Castonguay, A. Anticancer Activity and Catalytic Potential of Ruthenium(II)-Arene Complexes with N, O-Donor Ligands. *Inorg. Chem.* **2018**, *57*, 7558−7567.
(25) Chow, M. J.; Babak, M. V.; Tan, K. W.; Cheong, M. C.; Pastorin, G.; Gaiddon, C.; Ang, W. H. Induction of the Endoplasmic Reticulum Stress Pathway by Highly Cytotoxic Organoruthenium Schiff-Base Complexes. *Mol. Pharmaceutics* **2018**, *15*, 3020−3031.
(26) Brissos, R. F.; Clavero, P.; Gallen, A.; Grabulosa, A.; Barrios, L. A.; Caballero, A. B.; Korrodi-Gregorio, L.; Perez-Tomas, R.; Muller, G.; Soto-Cerrato, V.; Gamez, P. Highly Cytotoxic Ruthenium(II)-Arene Complexes from Bulky 1-Pyrenylphosphane Ligands. *Inorg. Chem.* **2018**, *57*, 14786−14797.
(27) Ma, W.; Guo, L.; Tian, Z.; Zhang, S.; He, X.; Li, J.; Yang, Y.; Liu, Z. Rhodamine-modified fluorescent half-sandwich iridium and ruthenium complexes: potential application as bioimaging and anticancer agents. *Dalton Trans.* **2019**, *48*, 4788−4793.
(28) Chen, F.; Romero-Canelon, I.; Soldevila-Barreda, J. J.; Song, J.-I.; Coverdale, J. P. C.; Clarkson, G. J.; Kasparkova, J.; Habtemariam, A.; Wills, M.; Brabec, V.; Sadler, P. J. Transfer Hydrogenation and Antiproliferative Activity of Tethered Half-Sandwich Organoruthenium Catalysts. *Organometallics* **2018**, *37*, 1555−1566.
(29) Hartinger, C. G.; Zorbas-Seifried, S.; Jakupec, M. A.; Kynast, B.; Zorbas, H.; Keppler, B. K. From bench to bedside - preclinical and early clinical development of the anticancer agent indazolium trans-[tetrachlorobis(1H-indazole)ruthenate(III)] (KP1019 or FFC14A). *J. Inorg. Biochem.* **2006**, *100*, 891−904.
(30) Bergamo, A.; Sava, G. Ruthenium complexes can target determinants of tumor malignancy. *Dalton Trans.* **2007**, 1267−1272.
(31) Bergamo, A.; Gaiddon, C.; Schellens, J. H. M.; Beijnen, J. H.; Sava, G. Approaching tumour therapy beyond platinum drugs: Status of the art and perspectives of ruthenium drug candidates. *J. Inorg. Biochem.* **2012**, *106*, 90−99.
(32) Trondl, R.; Heffeter, P.; Kowol, C. R.; Jakupec, M. A.; Berger, W.; Keppler, B. K. NKP-1339, the first ruthenium-based anticancer drug on the edge to clinical application. *Chem. Sci.* **2014**, *5*, 2925−2932.
(33) Kuhn, P. S.; Pichler, V.; Roller, A.; Hejl, M.; Jakupec, M. A.; Kandioller, W.; Keppler, B. K. Improved reaction conditions for the synthesis of new NKP-1339 derivatives and preliminary investigations on their anticancer potential. *Dalton Trans.* **2015**, *44*, 659−668.
(34) Shi, G.; Monro, S.; Hennigar, R.; Colpitts, J.; Fong, J.; Kasimova, K.; Yin, H.; DeCoste, R.; Spencer, C.; Chamberlain, L.; Mandel, A.; Lilge, L.; McFarland, S. A. Ru(II) dyads derived from α-oligothiophenes: A new class of potent and versatile photosensitizers for PDT. *Coord. Chem. Rev.* **2015**, *282*−*283*, 127−138.
(35) Schluga, P.; Hartinger, C. G.; Egger, A.; Reisner, E.; Galanski, M.; Jakupec, M. A.; Keppler, B. K. Redox behavior of tumor-inhibiting ruthenium(III) complexes and effects of physiological reductants on their binding to GMP. *Dalton Trans.* **2006**, 1796−1802.
(36) Chen, H.; Parkinson, J. A.; Parsons, S.; Coxall, R. A.; Gould, R. O.; Sadler, P. J. Organometallic Ruthenium(II) Diamine Anticancer Complexes: Arene-Nucleobase Stacking and Stereospecific Hydrogen-Bonding in Guanine Adducts. *J. Am. Chem. Soc.* **2002**, *124*, 3064−3082.
(37) Peacock, A. F. A.; Habtemariam, A.; Fernandez, R.; Walland, V.; Fabbiani, F. P. A.; Parsons, S.; Aird, R. E.; Jodrell, D. I.; Sadler, P. J. Tuning the Reactivity of Osmium(II) and Ruthenium(II) Arene Complexes under Physiological Conditions. *J. Am. Chem. Soc.* **2006**, *128*, 1739−1748.
(38) Wang, F.; Habtemariam, A.; van der Geer, E. P. L.; Fernandez, R.; Melchart, M.; Deeth, R. J.; Aird, R.; Guichard, S.; Fabbiani, F. P. A.; Lozano-Casal, P.; Oswald, I. D. H.; Jodrell, D. I.; Parsons, S.; Sadler, P. J. Controlling ligand substitution reactions of organometallic complexes: Tuning cancer cell cytotoxicity. *Proc. Natl. Acad. Sci. U. S. A.* **2005**, *102*, 18269−18274.
(39) Peacock, A. F. A.; Sadler, P. J. Medicinal organometallic chemistry: designing metal arene complexes as anticancer agents. *Chem. - Asian J.* **2008**, *3*, 1890−1899.
(40) Bugarcic, T.; Habtemariam, A.; Stepankova, J.; Heringova, P.; Kasparkova, J.; Deeth, R. J.; Johnstone, R. D. L.; Prescimone, A.; Parkin, A.; Parsons, S.; Brabec, V.; Sadler, P. J. The Contrasting Chemistry and Cancer Cell Cytotoxicity of Bipyridine and Bipyridinediol Ruthenium(II) Arene Complexes. *Inorg. Chem.* **2008**, *47*, 11470−11486.
(41) Yan, Y. K.; Melchart, M.; Habtemariam, A.; Sadler, P. J. Organometallic chemistry, biology and medicine: ruthenium arene anticancer complexes. *Chem. Commun.* **2005**, 4764−4776.

https://dx.doi.org/10.1021/acs.inorgchem.0c00694
Inorg. Chem. XXXX, XXX, XXX−XXX

(42) Habtemariam, A.; Melchart, M.; Fernandez, R.; Parsons, S.; Oswald, I. D. H.; Parkin, A.; Fabbiani, F. P. A.; Davidson, J. E.; Dawson, A.; Aird, R. E.; Jodrell, D. I.; Sadler, P. J. Structure-Activity Relationships for Cytotoxic Ruthenium(II) Arene Complexes Containing N, N-, N, O-, and O, O-Chelating Ligands. *J. Med. Chem.* **2006**, *49*, 6858−6868.
(43) Corte-Real, L.; Teixeira, R. G.; Girio, P.; Comsa, E.; Moreno, A.; Nasr, R.; Baubichon-Cortay, H.; Avecilla, F.; Marques, F.; Robalo, M. P.; Mendes, P.; Ramalho, J. P. P.; Garcia, M. H.; Falson, P.; Valente, A. Methyl-cyclopentadienyl Ruthenium Compounds with 2,2′-Bipyridine Derivatives Display Strong Anticancer Activity and Multidrug Resistance Potential. *Inorg. Chem.* **2018**, *57*, 4629−4639.
(44) Zeng, L.; Gupta, P.; Chen, Y.; Wang, E.; Ji, L.; Chao, H.; Chen, Z.-S. The development of anticancer ruthenium(II) complexes: from single molecule compounds to nanomaterials. *Chem. Soc. Rev.* **2017**, *46*, 5771−5804.
(45) Antonarakis, E. S.; Emadi, A. Ruthenium-based chemotherapeutics: are they ready for prime time? *Cancer Chemother. Pharmacol.* **2010**, *66*, 1−9.
(46) Morris, R. E.; Aird, R. E.; del Socorro Murdoch, P.; Chen, H.; Cummings, J.; Hughes, N. D.; Parsons, S.; Parkin, A.; Boyd, G.; Jodrell, D. I.; Sadler, P. J. Inhibition of Cancer Cell Growth by Ruthenium(II) Arene Complexes. *J. Med. Chem.* **2001**, *44*, 3616−3621.
(47) Renfrew, A. K. Transition metal complexes with bioactive ligands: mechanisms for selective ligand release and applications for drug delivery. *Metallomics* **2014**, *6*, 1324−1335.
(48) Romero-Canelon, I.; Pizarro, A. M.; Habtemariam, A.; Sadler, P. J. Contrasting cellular uptake pathways for chlorido and iodido iminopyridine ruthenium arene anticancer complexes. *Metallomics* **2012**, *4*, 1271−1279.
(49) Romero-Canelon, I.; Salassa, L.; Sadler, P. J. The Contrasting Activity of Iodido versus Chlorido Ruthenium and Osmium Arene Azo- and Imino-pyridine Anticancer Complexes: Control of Cell Selectivity, Cross-Resistance, p53 Dependence, and Apoptosis Pathway. *J. Med. Chem.* **2013**, *56*, 1291−1300.
(50) Pantic, D. N.; Aranđelovic, S.; Radulovic, S.; Roller, A.; Arion, V. B.; Grguric-Sipka, S. Synthesis, characterisation and cytotoxic activity of organoruthenium(II)-halido complexes with 1H-benzimidazole-2-carboxylic acid. *J. Organomet. Chem.* **2016**, *819*, 61−68.
(51) Lord, R. M.; Allison, S. J.; Rafferty, K.; Ghandhi, L.; Pask, C. M.; McGowan, P. C. Cytotoxic hydrogen bridged ruthenium quinaldamide complexes showing induced cancer cell death by apoptosis. *Dalton Trans.* **2016**, *45*, 13196−13203.
(52) Bhattacharyya, S.; Purkait, K.; Mukherjee, A. Ruthenium(II) p-cymene complexes of a benzimidazole-based ligand capable of VEGFR2 inhibition: hydrolysis, reactivity and cytotoxicity studies. *Dalton Trans.* **2017**, *46*, 8539−8554.
(53) Wang, X.; Li, J.; Dong, G.; Yue, J. The endogenous substrates of brain CYP2D. *Eur. J. Pharmacol.* **2014**, *724*, 211−218.
(54) Broadley, K. J. The vascular effects of trace amines and amphetamines. *Pharmacol. Ther.* **2010**, *125*, 363−375.
(55) Hauptmann, N.; Grimsby, J.; Shih, J. C.; Cadenas, E. The metabolism of tyramine by monoamine oxidase A/B causes oxidative damage to mitochondrial DNA. *Arch. Biochem. Biophys.* **1996**, *335*, 295−304.
(56) El Brahmi, N.; El Kazzouli, S.; Mignani, S. M.; Essassi, E. M.; Aubert, G.; Laurent, R.; Caminade, A.-M.; Bousmina, M. M.; Cresteil, T.; Majoral, J.-P. Original Multivalent Copper(II)-Conjugated Phosphorus Dendrimers and Corresponding Mononuclear Copper(II) Complexes with Antitumoral Activities. *Mol. Pharmaceutics* **2013**, *10*, 1459−1464.
(57) Mignani, S.; El Brahmi, N.; Eloy, L.; Poupon, J.; Nicolas, V.; Steinmetz, A.; El Kazzouli, S.; Bousmina, M. M.; Blanchard-Desce, M.; Caminade, A.-M.; Majoral, J.-P.; Cresteil, T. Anticancer copper(II) phosphorus dendrimers are potent proapoptotic Bax activators. *Eur. J. Med. Chem.* **2017**, *132*, 142−156.
(58) Ottaviani, M. F.; El Brahmi, N.; Cangiotti, M.; Coppola, C.; Buccella, F.; Cresteil, T.; Mignani, S.; Caminade, A. M.; Costes, J. P.; Majoral, J. P. Comparative EPR studies of Cu(II)-conjugated phosphorous-dendrimers in the absence and presence of normal and cancer cells. *RSC Adv.* **2014**, *4*, 36573−36583.
(59) Mignani, S. M.; El Brahmi, N.; El Kazzouli, S.; Laurent, R.; Ladeira, S.; Caminade, A.-M.; Pedziwiatr-Werbicka, E.; Szewczyk, E. M.; Bryszewska, M.; Bousmina, M. M.; Cresteil, T.; Majoral, J.-P. Original Multivalent Gold(III) and Dual Gold(III)-Copper(II) Conjugated Phosphorus Dendrimers as Potent Antitumoral and Antimicrobial Agents. *Mol. Pharmaceutics* **2017**, *14*, 4087−4097.
(60) Li, Y.-G.; Shi, D.-H.; Zhu, H.-L.; Yan, H.; Ng, S. W. Transition metal complexes (M = Cu, Ni and Mn) of Schiff-base ligands: Syntheses, crystal structures, and inhibitory bioactivities against urease and xanthine oxidase. *Inorg. Chim. Acta* **2007**, *360*, 2881−2889.
(61) Khandelwal, S.; Zamader, A.; Nagayach, V.; Dolui, D.; Mir, A. Q.; Dutta, A. Inclusion of Peripheral Basic Groups Activates Dormant Cobalt-Based Molecular Complexes for Catalytic H2 Evolution in Water. *ACS Catal.* **2019**, *9*, 2334−2344.
(62) Perrin, D. D.; Armarego, W. L. F. *Purification of Laboratory Chemicals*, 3rd ed.; Butterworth-Heinemann, 1988; p 391 pp.
(63) Bennett, M. A.; Huang, T. N.; Matheson, T. W.; Smith, A. K. (η6-Hexamethylbenzene)ruthenium complexes. *Inorg. Synth.* **1982**, *21*, 74−8.
(64) Acharya, S.; Maji, M.; Ruturaj; Purkait, K.; Gupta, A.; Mukherjee, A. Synthesis, Structure, Stability, and Inhibition of Tubulin Polymerization by Ru(II)-p-Cymene Complexes of Trimethoxyaniline-Based Schiff Bases. *Inorg. Chem.* **2019**, *58*, 9213−9224.
(65) Kubanik, M.; Holtkamp, H.; Sohnel, T.; Jamieson, S. M. F.; Hartinger, C. G. Impact of the Halogen Substitution Pattern on the Biological Activity of Organoruthenium 8-Hydroxyquinoline Anticancer Agents. *Organometallics* **2015**, *34*, 5658−5668.
(66) Schmidlehner, M.; Pichler, V.; Roller, A.; Jakupec, M. A.; Kandioller, W.; Keppler, B. K. Organometallic complexes of (thio)-allomaltol-based Mannich-products: Synthesis, stability and preliminary biological investigations. *J. Organomet. Chem.* **2015**, *782*, 69−76.
(67) Deer, E. L.; Gonzalez-Hernandez, J.; Coursen, J. D.; Shea, J. E.; Ngatia, J.; Scaife, C. L.; Firpo, M. A.; Mulvihill, S. J. Phenotype and genotype of pancreatic cancer cell lines. *Pancreas* **2010**, *39*, 425−435.
(68) Ang, W. H.; Daldini, E.; Scolaro, C.; Scopelliti, R.; Juillerat-Jeannerat, L.; Dyson, P. J. Development of Organometallic Ruthenium-Arene Anticancer Drugs That Resist Hydrolysis. *Inorg. Chem.* **2006**, *45*, 9006−9013.
(69) Dougan, S. J.; Melchart, M.; Habtemariam, A.; Parsons, S.; Sadler, P. J. Phenylazo-pyridine and phenylazo-pyrazole chlorido ruthenium(II) arene complexes: Arene loss, aquation, and cancer cell cytotoxicity. *Inorg. Chem.* **2006**, *45*, 10882−10894.
(70) Dougan, S. J.; Habtemariam, A.; McHale, S. E.; Parsons, S.; Sadler, P. J. Catalytic organometallic anticancer complexes. *Proc. Natl. Acad. Sci. U. S. A.* **2008**, *105*, 11628−11633.
(71) Purkait, K.; Karmakar, S.; Bhattacharyya, S.; Chatterjee, S.; Dey, S. K.; Mukherjee, A. A hypoxia efficient imidazole-based RuII arene anticancer agent resistant to deactivation by glutathione. *Dalton Trans.* **2015**, *44*, 5969−5973.
(72) Purkait, K.; Ruturaj; Mukherjee, A.; Gupta, A. ATP7B Binds Ruthenium(II) p-Cymene Half-Sandwich Complexes: Role of Steric Hindrance and Ru-I Coordination in Rescuing the Sequestration. *Inorg. Chem.* **2019**, *58*, 15659−15670.
(73) Bugarcic, T.; Habtemariam, A.; Deeth, R. J.; Fabbiani, F. P. A.; Parsons, S.; Sadler, P. J. Ruthenium(II) Arene Anticancer Complexes with Redox-Active Diamine Ligands. *Inorg. Chem.* **2009**, *48*, 9444−9453.
(74) Linares, F.; Galindo, M. A.; Galli, S.; Romero, M. A.; Navarro, J. A. R.; Barea, E. Tetranuclear Coordination Assemblies Based on Half-Sandwich Ruthenium(II) Complexes: Noncovalent Binding to DNA and Cytotoxicity. *Inorg. Chem.* **2009**, *48*, 7413−7420.
(75) Pettinari, R.; Pettinari, C.; Marchetti, F.; Skelton, B. W.; White, A. H.; Bonfili, L.; Cuccioloni, M.; Mozzicafreddo, M.; Cecarini, V.; Angeletti, M.; Nabissi, M.; Eleuteri, A. M. Arene-Ruthenium(II) Acylpyrazolonato Complexes: Apoptosis-Promoting Effects on Human Cancer Cells. *J. Med. Chem.* **2014**, *57*, 4532−4542.

https://dx.doi.org/10.1021/acs.inorgchem.0c00694
Inorg. Chem. XXXX, XXX, XXX−XXX

(76) Wang, H.-Y.; Qian, Y.; Wang, F.-X.; Habtemariam, A.; Mao, Z.-W.; Sadler, P. J.; Liu, H.-K. Ruthenium(II)-Arene Metallacycles: Crystal Structures, Interaction with DNA, and Cytotoxicity. *Eur. J. Inorg. Chem.* **2017**, *2017*, 1792−1799.
(77) Chelopo, M. P.; Pawar, S. A.; Sokhela, M. K.; Govender, T.; Kruger, H. G.; Maguire, G. E. M. Anticancer activity of ruthenium(II) arene complexes bearing 1,2,3,4-tetrahydroisoquinoline amino alcohol ligands. *Eur. J. Med. Chem.* **2013**, *66*, 407−414.
(78) Biancalana, L.; Pratesi, A.; Chiellini, F.; Zacchini, S.; Funaioli, T.; Gabbiani, C.; Marchetti, F. Ruthenium arene complexes with triphenylphosphane ligands: cytotoxicity towards pancreatic cancer cells, interaction with model proteins, and effect of ethacrynic acid substitution. *New J. Chem.* **2017**, *41*, 14574−14588.
(79) Kurzwernhart, A.; Kandioller, W.; Baechler, S.; Bartel, C.; Martic, S.; Buczkowska, M.; Muehlgassner, G.; Jakupec, M. A.; Kraatz, H.-B.; Bednarski, P. J.; Arion, V. B.; Marko, D.; Keppler, B. K.; Hartinger, C. G. Structure-Activity Relationships of Targeted RuII(η^6-*p*-Cymene) Anticancer Complexes with Flavonol-Derived Ligands. *J. Med. Chem.* **2012**, *55*, 10512−10522.
(80) Boege, M.; Fowelin, C.; Bednarski, P.; Heck, J. Diaminohexopyranosides as Ligands in Half-Sandwich Ruthenium(II), Rhodium(III), and Iridium(III) Complexes. *Organometallics* **2015**, *34*, 1507−1521.
(81) Aliende, C.; Perez-Manrique, M.; Jalon, F. A.; Manzano, B. R.; Rodriguez, A. M.; Cuevas, J. V.; Espino, G.; Martinez, M. A.; Massaguer, A.; Gonzalez-Bartulos, M.; de Llorens, R.; Moreno, V. Preparation of new half sandwich ruthenium arene complexes with aminophosphines as potential chemotherapeutics. *J. Inorg. Biochem.* **2012**, *117*, 171−188.
(82) Adhikari, S.; Hussain, O.; Phillips, R. M.; Kollipara, M. R. Half-sandwich d6 metal complexes comprising of 2-substituted-1,8-naphthyridine ligands with unexpected bonding modes: Synthesis, structural and anti-cancer studies. *J. Organomet. Chem.* **2018**, *854*, 27−37.
(83) de la Cueva-Alique, I.; Sierra, S.; Munoz-Moreno, L.; Perez-Redondo, A.; Bajo, A. M.; Marzo, I.; Gude, L.; Cuenca, T.; Royo, E. Biological evaluation of water soluble arene Ru(II) enantiomers with amino-oxime ligands. *J. Inorg. Biochem.* **2018**, *183*, 32−42.
(84) Adhikari, S.; Hussain, O.; Phillips, R. M.; Kaminsky, W.; Kollipara, M. R. Synthesis, structural and chemosensitivity studies of arene d^6 metal complexes having N-phenyl-N'-(pyridyl/pyrimidyl)-thiourea derivatives. *Appl. Organomet. Chem.* **2018**, *32*, No. e4362.
(85) Adhikari, S.; Hussain, O.; Phillips, R. M.; Kaminsky, W.; Kollipara, M. R. Neutral and cationic half-sandwich arene d^6 metal complexes containing pyridyl and pyrimidyl thiourea ligands with interesting bonding modes: Synthesis, structural and anti-cancer studies. *Appl. Organomet. Chem.* **2018**, *32*, No. e4476.
(86) Palepu, N. R.; Adhikari, S.; J, R. P.; Verma, A. K.; Shepherd, S. L.; Phillips, R. M.; Kaminsky, W.; Kollipara, M. R. Half-sandwich ruthenium, rhodium and iridium complexes featuring oxime ligands: Structural studies and preliminary investigation of in vitro and in vivo anti-tumour activities. *Appl. Organomet. Chem.* **2017**, *31*, No. e3640.
(87) Bromann, P. A.; Korkaya, H.; Courtneidge, S. A. The interplay between Src family kinases and receptor tyrosine kinases. *Oncogene* **2004**, *23*, 7957−7968.
(88) Lee, Y.-J.; Cho, H.-N.; Soh, J.-W.; Jhon, G. J.; Cho, C.-K.; Chung, H.-Y.; Bae, S.; Lee, S.-J.; Lee, Y.-S. Oxidative stress-induced apoptosis is mediated by ERK1/2 phosphorylation. *Exp. Cell Res.* **2003**, *291*, 251−266.
(89) Massague, J. G1 cell-cycle control and cancer. *Nature* **2004**, *432*, 298−306.
(90) Kroemer, G.; Reed, J. C. Mitochondrial control of cell death. *Nat. Med.* **2000**, *6*, 513−519.

https://dx.doi.org/10.1021/acs.inorgchem.0c00694
Inorg. Chem. XXXX, XXX, XXX−XXX